Experimental Studies of Hypersonic Shock-Wave Boundary-Layer Interactions

by

Frank K. Lu
Mechanical and Aerospace Engineering Department
University of Texas at Arlington
Arlington, Texas 76019-0018

Final Report

submitted to

Dr. John P. Weidner
Hypersonic Propulsion Branch, MS-168
NASA Langley Research Center
Hampton, VA 23665

Grant NAG 1-891

September 10, 1992

Two classes of shock-wave boundary-layer interactions were studied experimentally in a shock tunnel in which a low Reynolds number, turbulent flow at Mach 8 was developed on a cold, flat test surface. The two classes of interactions were (*a*) a swept interaction generated by a wedge ("fin") mounted perpendicularly on the flat plate and (*b*) a two-dimensional, unseparated interaction induced by a shock impinging near an expansion corner. The swept interaction, with wedge angles of 5–20 degrees, was separated and there was also indication that the strongest interactions possessed secondary separation zones. The interaction spread out extensively from the inviscid shock location although no indication of quasi-conical symmetry was evident. The surface pressure from the upstream influence to the inviscid shock was relatively low compared to the inviscid downstream value but it rose rapidly past the inviscid shock location. However, the surface pressure did not reach the downstream inviscid value and reasons were proposed for this anomalous behavior compared to strongly separated, supersonic interactions. The second class of interactions involved weak shocks impinging near small expansion corners. As a prelude to studying this interaction, a hypersonic similarity parameter was identified for the pure, expansion corner flow. The expansion corner severely damped out surface pressure fluctuations. When a shock impinged upstream of the corner, no significant changes to the surface pressure were found as compared to the case when the shock impinged on a flat plate. But when the shock impinged downstream of the corner a close coupling existed between the two wave systems, unlike the supersonic case. This close coupling modified the upstream influence. Regardless of whether the shock impinged ahead or behind the corner, the downstream region was affected by the close coupling between the shock and the expansion. Not only was the mean pressure distribution modified but the unsteadiness in the surface pressure was reduced compared to the flat-plate case.

Contents

List of Figures

1 Introduction

In the present development of airbreathing hypersonic vehicles, a critical problem that needs to be addressed is the understanding and solution of complex viscous-inviscid interaction flowfields not previously encountered.[1] Interactions such as those between shock waves and turbulent boundary layers are particularly important in determining the performance of engine inlets. The highly complex inlet flowfield has to be properly understood before the performance of the rest of the scramjet propulsion system can be predicted with confidence. The challenge in predicting the hypersonic inlet flowfield using latest generation supercomputers and state-of-the-art techniques has proven to be a particularly daunting one with a recurring question that so far has not been adequately answered: how accurate and realistic are the computations?[2] One recourse is to compare the computations with detailed and carefully conducted experiments. The situation regarding the experimental database is, however, not particularly rosy. A recent compilation[3] has revealed that although there is a large number of hypersonic shock boundary-layer experiments, the quality of these experiments is varied. A set of stringent criteria reduced 105 candidate hypersonic studies to only five. Undoubtedly, high-quality benchmark experiments are required. Such experiments also serve to improve understanding of the complex physical processes governing the interaction which at times lead to discovery of new phenomena.

Clearly, the current database and physical understanding for modeling high-speed viscous-inviscid interactions is woefully lacking. A body of work at supersonic Mach numbers has however been built up over the past two decades.[4–7] The knowledge unfortunately becomes deficient at hypersonic Mach numbers[3] where there is a dependence on semi-empirical correlations for design purposes.[8,9] To partly address this deficiency, an exploratory program in hypersonic shock boundary-layer interactions was initiated by the University of Texas at Arlington. Two configurations were examined. The first depicted in Fig. 1 is of a sharp-wedged shock generator ("fin") mounted perpendicularly to a flat test surface. A semi-infinite, dimensionless, three-dimensional interaction[6] is generated between the shock and the turbulent boundary layer developing over the surface. The second depicted in Fig. 2 is a two-dimensional shock impinging near an expansion corner. Moreover, due to the lack of data on an expansion-corner flow, effort was also expended toward understanding this flow. In the subsequent sections, experimental procedures, results of the present study, and pertinent observations and conclusions will be presented.

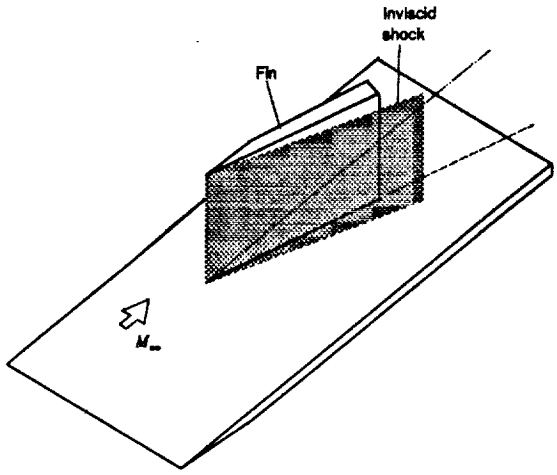

Figure 1: Schematic of "fin" configuration.

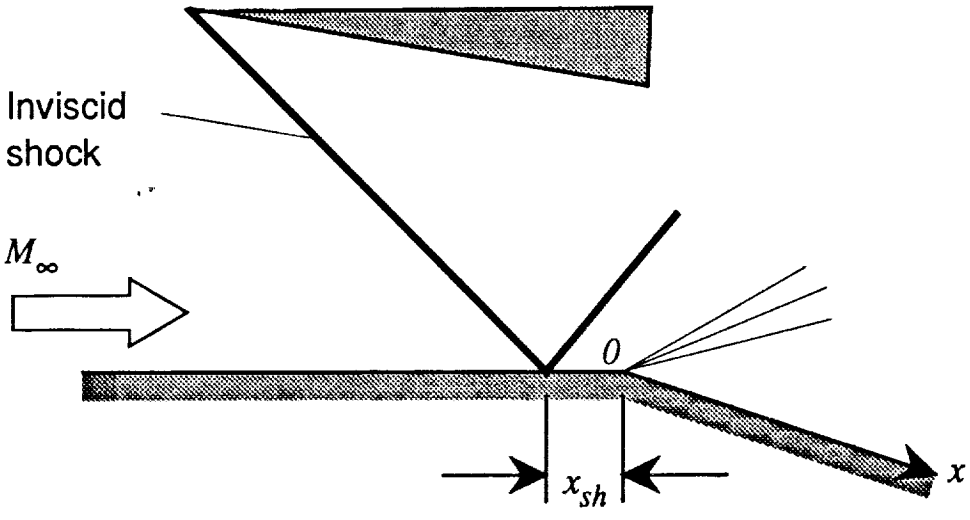

Figure 2: Schematic of shock impingement near expansion corner.

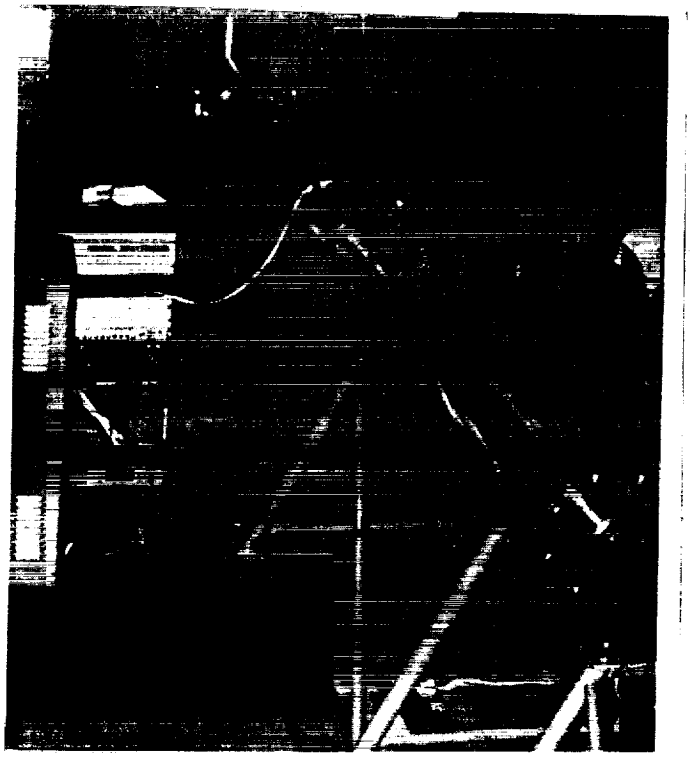

Figure 3: Shock tunnel facility.

2 Experimental Methods

2.1 Test Facility

The experiments were performed in the University of Texas at Arlington's Hypersonic Shock Tunnel Facility located in the Aerodynamics Research Center (ARC).[10] A partial view of the shock tunnel is shown in Fig. 3. The tunnel was of conventional design and, as can be seen in sequence from the top of the figure, consisted of a test section, a nozzle and a shock tube. Only part of the driven section of the shock tube is visible in Fig. 3. Partly hidden from view is the diffuser which protruded out of the far wall into a vacuum tank outside. Not visible are a double-diaphragm section and the driver section of the shock tube. In addition to the tunnel itself, the figure also shows the data acquisition crate on the left and the vacuum system on the right. A brief description of the major components of the facility is now provided.

2.1.1 Shock Tube

The shock tube consisted of a high-pressure driver tube connected to a driven tube by a double-diaphragm section. The driver tube of 152-mm (6-in.) bore was 3 m (10 ft) long. The driven tube also of 152 mm (6 in.) bore was made of three 2.7-m (9-ft) segments to facilitate installation and disassembly when necessary for cleaning.

The driver tube, the diaphragm section and the driven tube were bolted together with two 267-mm (10.5-in.) square diaphragms enclosing a plenum. The double-diaphragm arrangement allowed precise control of diaphragm rupture. The diaphragm material was 10-gauge (3.42 mm, 0.1345 in.) hot-rolled steel sheets (ASTM

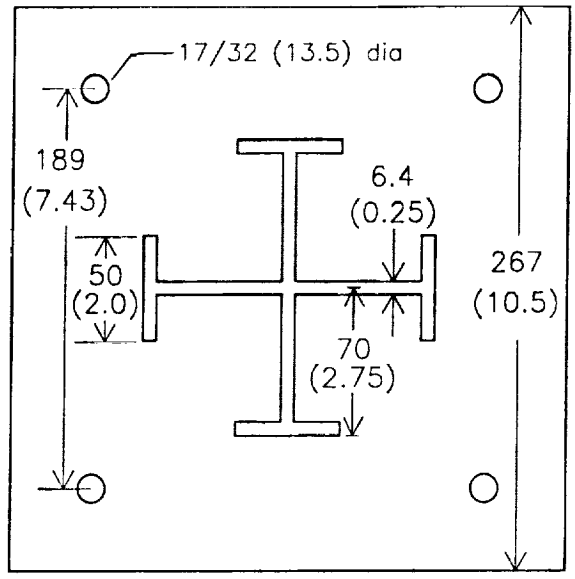

Figure 4: Diaphragm scoring pattern.

A36) chosen because of its low cost. To ensure clean rupture with minimum fragmentation while also providing a degree of controllability, a pattern was scored onto the diaphragm. A *cross potent*[11] pattern 3.18 mm (0.125 in.) wide and 0.5 ± 0.1 mm (0.020 ± 0.005 in.) deep was found to give optimal diaphragm opening for the pressures encountered in the present study, Fig. 4. The scored diaphragms failed when they were subjected to a pressure difference of about 13 MPa (2,000 psi), which was larger than the initial pressure difference that the diaphragms were subjected to in the shock tube. The diaphragms were placed in the tunnel with the scoring pattern facing downstream and they generally "petaled" without fragmentation. Sometimes, the petals faced upstream or were curled after rupture. These were likely due to shock reflections within the shock tube. Further, in the extremely unlikely occurrence of fragmentation, the few fragments tended to be small and were trapped in the driven tube. These small fragments were cleaned out in preparation for the next run.

2.1.2 Nozzle, Test Section and Diffuser

A 7.5° half-angle conical nozzle with interchangeable throat inserts enabled test Mach numbers of 5 through 16 to be obtained. The exit diameter of this nozzle was 336 mm (13.25 in.). A Mach 8 throat insert was used for the experiments. A secondary diaphragm made of 0.127-mm (0.005-in.) thick aluminum sheet was located in the nozzle throat region and was used to separate the driven-tube gas from that in the test section. The secondary diaphragm was not scored. The test section was of an enclosed free-jet design and was 536 mm (21.1 in.) long and 440 mm (17.5 in.) in diameter. The nozzle and the diffuser both protruded slightly into the test section. Downstream of the diffuser was a receiver tank.

2.1.3 Pneumatic Systems

The ARC's high-pressure system[12] supplied dried air at 14.5 MPa (2,100 psi) which was then boosted to 31 MPa (4,500 psi) and stored. The stored air was regulated to lower pressure via a system of manual and remote-control valves when charging the driver and driven tubes.[13] In addition to the high-pressure system, two vacuum pumps were used to evacuate the driven tube, and the test section and vacuum tank. A custom-made pressure relief valve was incorporated into the vacuum tank to protect the 0–35 kPa (0–5 psia) transducers used for the experiments from overpressure damage. This valve consisted of a circular plate sealed tightly against a 76 mm (3 in.) pipe flange when the vacuum tank was evacuated. The seal was broken when the pressure in the vacuum tank exceeded atmospheric, causing the circular plate to pop from the flange and move along guide rods. After all pressure was relieved, the valve was manually closed for the next run.

2.1.4 Data Acquisition System, Instrumentation and Diagnostics

The data acquisition system consisted of a 286-type host computer connected to eight digitizers which simultaneously acquired data at one million samples per second. In front of the digitizers were eight external instrumentation amplifier-filter combinations operated with a gain of 500 and a bandwidth of 100 kHz. The data acquisition system was connected to the computer via a pair of bus extenders since the computer was located in a reinforced control room over 30 m (100 ft) away.

The test surface was instrumented with flush-mounted Kulite XCS-093-5A (0–35 kPa, 0–5 psia) and XCS-093-50A (0–350 kPa, 0–50 psia) pressure transducers potted in place using silicone rubber sealant. The transducers were flushed with the test surface to better than $\pm 0.005\delta_o$. These transducers had Type "M" protective screens and sensing surfaces of 0.97 mm (0.038 in.) diameter. Natural frequencies quoted by the manufacturer were 100 kHz and 200 kHz respectively. In the data processing, digital filtering was used to set the upper frequency of the signals to 100 kHz, which also removed high-frequency transducer noise and which gave a signal-to-noise ratio of better than 10:1.

For these transducers, a static calibration sufficed for determining their sensitivities even though these transducers were used in dynamic situations.[14] But the drift and hysteresis of these transducers were significant, especially if the transducers were used to measure low pressures.[15] To reduce drift, the transducers were calibrated *in situ* during evacuation of the test section against an MKS Baratron Model 127A vacuum gauge, a capacitance-type manometer accurate to ± 7 Pa (± 0.001 psia) that is used widely as a secondary standard. Least-squares linear fits were made on the calibration data from which the transducers' sensitivities were obtained. About thirty minutes elapsed between a run and the calibration during which significant zero shift was encountered. The drift problem was overcome by "renulling" the transducers through comparing their outputs against the vacuum gauge prior to tunnel firing.

Subsequently, the acquired data were converted into engineering units, with the sensitivities obtained from calibration and the offsets obtained from the final renulling adjustment. The calibrations were checked continually throughout the daily test sequence and the transducers were re-calibrated if necessary. Other problems of piezoresistive transducers, namely, thermal zero shift and thermal sensitivity were negligible due to the short run times of the tests.

With only eight data-acquisition channels available, detailed surface pressure distributions were obtained with a number of runs. Seven channels were used to measure surface pressures through the interaction while the eighth was used to measure a reference pressure p_∞. For the fin interaction, this pressure was measured 17.3 mm (0.68 in. or $1.3\delta_o$) ahead of the fin apex at the flat-plate centerline while for the expansion corner interaction, it was measured 34.9 mm (1.375 in. or $2.6\delta_o$) ahead of the corner. The measured interaction pressures were normalized by the reference pressure to minimize the effects of run-to-run variations in pressure arising from difficulties in estimating the stagnation conditions due to uncertainty in estimating the shock Mach number. In other words, the variations in pressure were equivalent to a small Reynolds number effect. Unused orifices were plugged with dummy transducer replicas made from steel rods.

For the expansion corner experiments, an attempt was made to characterize the surface pressure fluctuations. The bandwidth of the data was about 2–100 kHz, the lower cutoff frequency being determined by the available test time of about 0.5 ms. About 60 percent of the rms fluctuations were captured within the data bandwidth.[16] Each data record possessed about 500 data points which were deemed adequate for statistical analyses. To check if the above statement was valid, a number of data records were divided into two halves and the mean and rms values of these halves were compared. The mean and rms values differed from one to twelve percent and on average differed by six percent. Therefore, it was thought that the amount of data per record was sufficient.

In analyzing the data, the transducer spatial and frequency resolution limits were considered. The 100-kHz transducer bandwidth severely limited the upper nondimensional frequency $f\delta/U_\infty$ to about unity which was low compared to previous dynamic measurements.[17] The frequency resolution was also compared with those of different investigations by using a reduced frequency $f\nu_w/U_\tau^2$. In the present experiments, $f\nu_w/U_\tau^2 \approx 0.008$ which was also comparatively low.[17] In addition to the bandwidth limitation, high frequency damping was also partly due to transducer size. A nondimensional transducer diameter $d^+ \equiv U_\tau\, d/\nu_w$ was used for examining the effects of transducer size on spatial resolution, d being the transducer diameter. In the present experiments, $d^+ \approx 200$ which was in the 50–500 range of most supersonic experiments.[17] It remained unclear how d^+, $f\delta/U_\infty$ or $f\nu_w/U_\tau^2$ could be used to provide proper estimates of transducer spatial and frequency resolutions at high Mach numbers. The inability to resolve the highest frequencies nevertheless meant that knowledge on the spectral behavior of the finest scales that adjusts rapidly down-

stream of the corner was missing. Finally, it may also be noted that no corrections were made to the data due to the transducer size.

A boundary-layer rake was used to survey the undisturbed boundary layer and the two-dimensional interactions generated by shock impingement near an expansion corner. The rake consisted of a 130-mm (5.125-in.) long, 57-mm (2.25-in.) high by 22-mm (0.875-in.) wide hollow housing with a streamlined nose. In front of the housing were machined two slots, 38 mm (1.5 in.) high by 3.2 mm (0.125 in. wide), on either side of the plane of symmetry. One of the slots was for an array of pitot probes and the other was for an array of thermocouples. A stack of three pitot probes and another stack of three thermocouple probes were fastened into a movable subhousing within the main housing. The probes protruded through the slots and could be moved in small albeit variable steps to build up a boundary-layer profile in about four runs. After positioning the probes, a set screw was tightened against the subhousing to lock the probes in place. The pitot probes for boundary-layer surveys were flattened as is typical. To obtain adequate response, Kulite transducers were placed 18 mm (0.7 in.) from the tube orifices. The thermocouples were exposed to the incoming stream and were used for estimating stagnation temperature using a heat transfer method.[18] Unfortunately, the thermocouple response was too slow for the stagnation temperature to be estimated accurately.

For fin interactions, surface oil-dot visualization was also explored. Surface flow visualization was successfully used in determining the surface topological features of swept interactions.[6] However, its application in short-duration facilities appears problematic and is rare. Successful implementations were reported in Refs. 19 and 20. An effort was therefore undertaken in the present research to develop the technique. A mixture of Dow-Corning "200" 20-centistoke silicone oil and powdered, colored classroom chalk provided the appropriate qualities of low viscosity and low vapor pressure that were needed. Special applicators with sharp pins in a 31.8 mm (0.125 in.) grid were built to dot the mixture on the test surface. The oil-dot technique was found to be more suited for a shock-tunnel environment than the oil-flow technique. This is because long streaks obtained in the oil-flow visualization technique did not form in the shock tunnel due to the short run times. Without visible streaks, the oil-flow technique would be of limited utility. Further, the pattern was somewhat damp at the end of a run and, if the oil-flow technique was used, there was a greater chance of ruining the pattern when it was being lifted up than if the oil-dot technique was used. After a run, the pattern was lifted using laminating sheets and pasted on a sheet of paper. Analysis could then be performed on the fullsize, undistorted patterns.

2.2 Models

2.2.1 Interaction Test Surface

The flat plate on which the boundary layer developed was made of stainless steel squares mounted on an aluminum base and a stainless steel frame as follows. A 12.7-

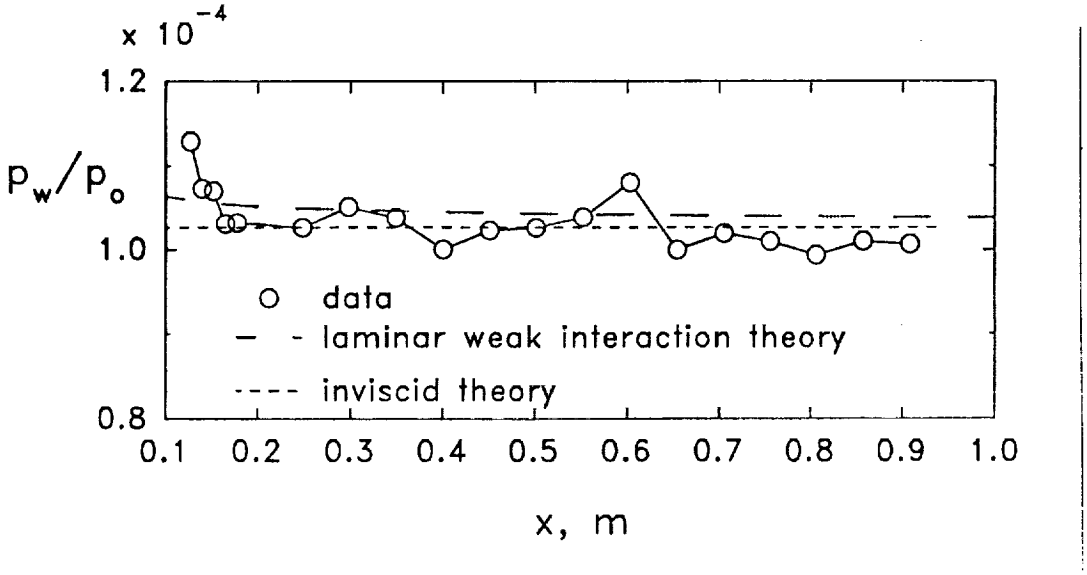

Figure 5: Surface pressure on flat plate.

mm (0.5-in.) thick aluminum base was hollowed out on top for instrumentation and ancilliary wiring, the wiring being channeled through a port in an end cap bolted to the rear. On this base were attached 12.7-mm (0.5-in.) thick, stainless steel plates 200 mm (8 in.) square. These plates had grooves lined with O-ring material and were butted against each other tightly to provide a smooth test surface. To maintain structural integrity, the leading-edge segment which had a 15°-sharp leading edge was usually not removed from the aluminum base. The flat-plate subassembly was mounted 50 mm (2 in.) below the tunnel centerline to avoid "wave focusing" in axisymmetric test sections.[21] "Skirts" made of 25-mm (1-in.) square stainless steel rods with pointed upward-curving tips were attached along both sides of the model, serving to prevent crossflow contamination from the lower surface.[22] The entire assembly was mounted onto a pedestal which in turn was bolted to the floor of the test section.

The flat plate was long enough to enable a turbulent boundary layer to develop through the test region. However, due to the limited length of the test section, the flat plate protruded into the nozzle and diffuser. Thus, the boundary layer developing over the flat plate was initially subjected to a favorable pressure gradient, Fig. 5.[23] Nonetheless, in the test region, starting at about 750 mm (29.5 in.) from the flat-plate leading edge, the surface pressure showed only an extremely slight, favorable longitudinal pressure gradient which can be safely ignored. Assuming that the undisturbed surface pressure was constant resulted in an average data scatter of about three percent which was within measurement accuracy.

2.2.2 Fins

The fin model was fabricated from aluminum plate. It had a 10°-sharp leading edge and was 152 mm (6 in.) long and 127 mm (5 in.) high to ensure that a dimensionless, semi-infinite swept interaction[6] was obtained. A rubber seal under the fin and a thin ribbon of silicone rubber sealant on the leeside of the fin prevented leakage. The fin tip was located 761 mm (29.95 in.) from the flat-plate leading edge and 38 mm (1.5 in.) from one of the flat-plate sides. The fin was clamped tightly to the flat plate and its angle of attack was set to $\alpha = 5$, 10, 15 and $20 \pm 0.1°$. The corresponding values of M_n were 1.51, 2.14, 2.85 and 3.58 with respective pressure ratios of $\xi_{12} = 2.48$, 5.19, 9.30 and 14.82.

It was thought that quasi-conical symmetry[24–26] may exist in a hypersonic, fin-induced interaction. Therefore, better resolution of the surface pressure would be obtained if measurements were made along arcs centered at the fin apex than in rows parallel or perpendicular to the incoming flow. In the present experiments, pressure taps were located along two arcs at $s = 114$ mm (4.5 in.) and 152 mm (6 in.) from the fin apex. The first tap was located at 2° from the incoming flow direction and subsequent taps were spaced at 4° intervals. A centerline tap 17.27 mm (0.68 in.) ahead of the fin apex was used to measure a reference pressure p_∞.

2.2.3 Expansion Corners

For experiments involving shock impingement near expansion corners, a sharp convex corner was located at 768 mm (30.25 in.) from the flat-plate leading edge. Surface pressures across the corner were measured from 38.1 mm (1.5 in.) upstream to 60.3 mm (2.375 in.) downstream using a row of flush-mounted pressure transducers in orifices offset from the centerline by 3.18 mm (0.125 in.) and spaced 6.35 mm (0.25 in.) or $0.47\delta_o$ apart.

In designing the expansion corners, it was thought that hypersonic similarity may exist between corner flows at different Mach numbers for given values of the parameter

$$K = M_\infty \alpha \tag{1}$$

where α is the corner angle in radians, this similarity being analogous to hypersonic similarity between slender bodies[27] and which was shown by Stollery and Bates[28] to be an important parameter for hypersonic turbulent flows. Thus, it was thought that the hypersonic experiments would be more revealing if they were performed with values of K comparable to those found in more numerous supersonic experiments. Such an expectation for a hypersonic flow meant small corner angles were necessary for the experiments. These angles were chosen as $\alpha = 2.5°$ and 4.25°, with corresponding values of $K = 0.35$ and 0.59 at Mach 8, and were machined to an accuracy of $\pm 0.1°$. (A combined supersonic-hypersonic similarity parameter $\alpha\sqrt{M_\infty^2 - 1}$ proposed by Van Dyke[29] was also examined but this parameter was found to be applicable to a restricted range of very small values of α only.)

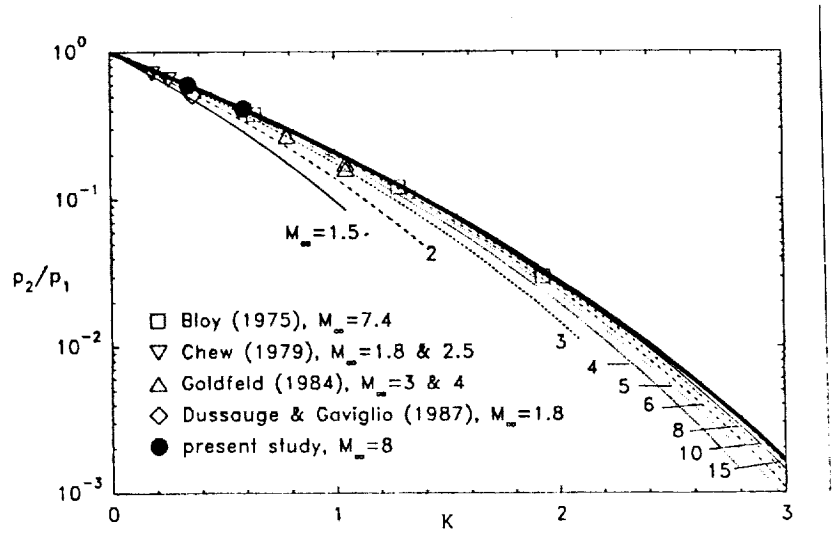

Figure 6: Hypersonic similarity of Prandtl-Meyer expansion.

The above assertion of K as a suitable similarity parameter was reinforced by the observation that the inviscid experimental conditions of different investigations[30–33] collapsed very well in terms of K, Fig. 6. This figure shows that the present values of α resulted in values of K that were within the range of previous supersonic experiments as mentioned above. Further, Fig. 6 also compares the pressure ratio as a function of K for Mach numbers from 1.5 through 15 with that for the hypersonic limit, this limiting case being shown as a thick line. In the limit of $M_\infty \to \infty$,[27]

$$\frac{p_2}{p_1} = \left(1 - \frac{\gamma - 1}{2} K\right)^{2\gamma/(\gamma-1)} . \tag{2}$$

Eqn. (2) is not limited to small expansion corners and, therefore, K is not restricted by the requirement of a small perturbation when used as a similarity parameter in the present application, unlike hypersonic slender-body theory. The excellent collapse of the pressure ratio through a wide range of K, even at quite low Mach numbers, may be attributed to the isentropic nature of the inviscid expansive flow. Nonetheless, for a given Mach number, there is a maximum value of K, corresponding to expansion to vacuum, this maximum value being smaller at lower Mach number. Further, the plots in Fig. 6 are of inviscid flows which can be turned through large corner angles. (The lower Mach number curves in Fig. 6 have been chopped below the maximum inviscid solution to reduce cluttering of the figure.) In a viscous flow, the boundary layer would separate at some critical corner angle, this angle being dependent on the Mach number, amongst other parameters. Thus, extremely strong hypersonic expansions that exist at large α, which are beyond the scope of the present investigation, will not have supersonic counterparts. These facts have to be borne in mind when comparing

data obtained at low Mach numbers with those obtained at higher Mach numbers. The appropriateness of K as a scaling parameter will be further discussed later.

2.2.4 Two-Dimensional, External Shock Generators

Shocks were impinged near the expansion corner by an external shock generator attached to an angle-of-attack adapter. The shock generator was fabricated out of aluminum plate and was 133 mm (5.25 in.) long, 178 mm (7.0 in.) wide and 12.7 mm (0.5 in.) thick. The leading-edge bevel was 25°. Due to the lack of previous studies of shock impingement near an expansion corner, it was thought that a systematic approach would be to study weak, unseparated interactions first. Hence, two adapters that set the angle of attack of the shock generator to $\beta = 2$ and $4° \pm 0.1°$ were used to mount the shock generator to a sting. In a Mach 8 stream, the two wedges generated weak shocks that produced inviscid pressure ratios of 1.46 and 2.09 respectively. The shock generator was located with its tip 76 mm above the test surface such that an inviscid shock would impinge the test surface at $\bar{x} = -1$, 0 and 1 from the corner.

2.3 Test Conditions

The shock tunnel was operated in the reflected shock, overtailored mode, also known as the "equilibrium interface" mode,[34] to obtain high Reynolds number, perfect gas conditions.[10] Unfortunately, this technique produced a useful test time of 0.3–0.5 ms in the present experiments, the actual test time being highly dependent on the initial unsteady wave system past the test configuration. To obtain the desired test conditions, the driver tube was charged to 24 MPa ± 1.5 percent (3,500 psia) and the double-diaphragm section to about 12 MPa (1,750 psia). The driven tube was charged to 280 kPa ± 1.3 percent (40 psia) after first being evacuated to remove moist ambient air. The test section, diffuser, and dump tank were evacuated to below 0.32 kPa (0.05 psia). The gas used throughout the tunnel was dried, unheated air.

Breaking the two diaphragms by venting the double-diaphragm section started the tunnel whereby a shock propagated into the driven tube and an unsteady expansion propagated into the driver tube. The actual speed of the shock as it propagated through the driven tube had to be known in order to estimate the test conditions. The shock speed was determined by timing the shock passage toward the end of the driven tube. The initial conditions produced a shock Mach number of 2.15 with a run-to-run variation of less than ±5 percent. The low shock Mach number ensured that real gas effects were negligibly small. The test conditions for the present study were an incoming freestream velocity of 1.24 km s^{-1} (4,080 ft/s), a nominal freestream Mach number of 8, stagnation pressure and temperature of $p_o = 5.38$ MPa (780 psia) and $T_o = 820$ K (1,480 °R) respectively and a Reynolds number of $Re = 10.2 \times 10^6$ m^{-1} (3.1 million/ft). This Reynolds number was deemed acceptable when compared with existing hypersonic facilities.[35,36] The static pressure and temperature under the above

conditions were 0.55 kPa (0.08 psia) and 59 K (107 °R) respectively and corresponded to conditions slightly above the air saturation line.[37] The flat plate was at room temperature ($T_w \approx 290$ K, 522 °R) and thus the experiments were performed under cold-wall conditions ($T_w/T_o \approx 0.35$). For flow past the 2.5° and 4.25° corners, the downstream inviscid conditions were static pressures and temperatures of 0.33 kPa (0.048 psia) and 51 K (92 °R), and 0.23 kPa (0.033 psia) and 46 K (83 °R) respectively. These conditions were close to but above the air saturation line.[37] The respective downstream Mach numbers were 8.65 and 9.15.

The low accuracy in estimating the shock Mach number was thought to be misleading because the accuracy was limited by the accuracy of resolving the shock fronts and was not due to poor control of the initial tunnel conditions. The five percent repeatability in the estimated shock Mach number between runs resulted in an estimated maximum scatter of thirteen percent, seven percent and twenty percent on the stagnation pressure and temperature, and Reynolds number respectively for the ensemble of runs. As discussed in Sect. 2.1.4 above, steps were taken to minimize the run-to-run variation through normalizing the surface pressure.

It is well known that the transition Reynolds number increases with Mach number. In hypersonic testing of turbulent boundary-layer flows, long models are, therefore, unavoidable. Artificially tripping the boundary layer to shorten the model was not suitable since disturbances caused by the trips would be convected for long distances downstream.[38] Using the correlations of Ref. 39, the boundary layer in the present experiments was deemed turbulent ahead of the corner location. Further, the undisturbed boundary layer was surveyed[23] and it was found to be nominally two-dimensional in the test region. From the pitot pressure profiles, the incoming boundary layer thickness was estimated at 13.5 ± 2 mm (0.53 ± 0.08 in). (It may be noted here that the use of the pitot pressure profile for estimating the boundary-layer edge is a practice recommended by Fernholz and Finley,[40] especially at high Mach numbers.) The undisturbed boundary layer possessed characteristics typical of low Reynolds number, turbulent flows, with $Re_\theta = 1800$–2300, and it possessed a negligible wake component. The lack of a wake component is evident in Fig. 7 which plots the velocity profiles in wall coordinates subjected to the Van Driest transformation.

A test flow of about 0.5 ms duration was established at the interaction region after a starting time of about 2 ms. The test time corresponded to a slug of test gas 0.6 m long. The interaction region along the expansion corner of about 0.2 m, or one-third the length of test gas, more than fulfilled the requirement for a fully-developed turbulent flow to exist.[41]

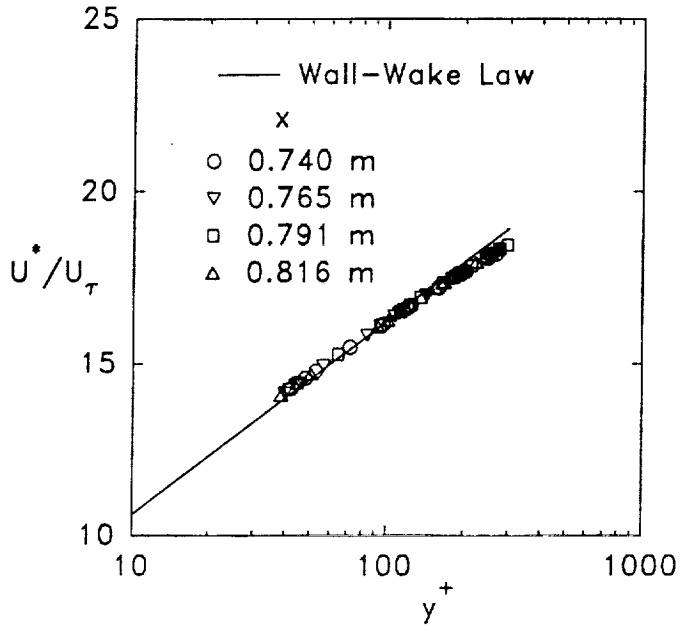

Figure 7: Transformed velocity profiles of undisturbed boundary layer in wall coordinates.

3 Results and Discussion

3.1 Fin Interactions

Oil-dot flow visualization traces are shown in Figs. 8–11. The fin and the inviscid shock locations are also shown in each trace. The dots were made using applicators which had one side cut to match the fin angle. In this way, the rows of dots were aligned with the incoming freestream direction to ease identification of the surface flow deflection. Fainter areas on the patterns were due to uneven application of the oil dots and were not interaction phenomena. Also, lines visible in some of the figures were seams in between pieces of tape used to lift the pattern. In Fig. 8, slight smearing of the pattern is evident from the short spanwise streaks in the region ahead of the fin. Smearing was caused by applying the oil too heavily. These artifacts of the technique, although distracting, did not pose serious problems in analyzing the traces.

For the pattern produced by the $\alpha = 5°$ interaction, the surface flow was deflected through a large angular extent compared to the inviscid shock. A distinct convergence line that would form if the streaks were merged for separated interaction was not seen in the pattern and this was likely due to the shortness of the streaks. Nonetheless, the interaction was deemed to be separated because the streaks were deflected to angles larger than β_o, a situation that occurs in separated, supersonic interactions. Additionally, the separation appeared to occur very close to the upstream influence line. The observed separation lent support to Korkegi's criterion,[42] which for Mach 8 predicts a fin angle for incipient separation of 2.2°. Also, it can be seen that the interaction "bowed" out very rapidly from the fin apex to produce a highly-swept

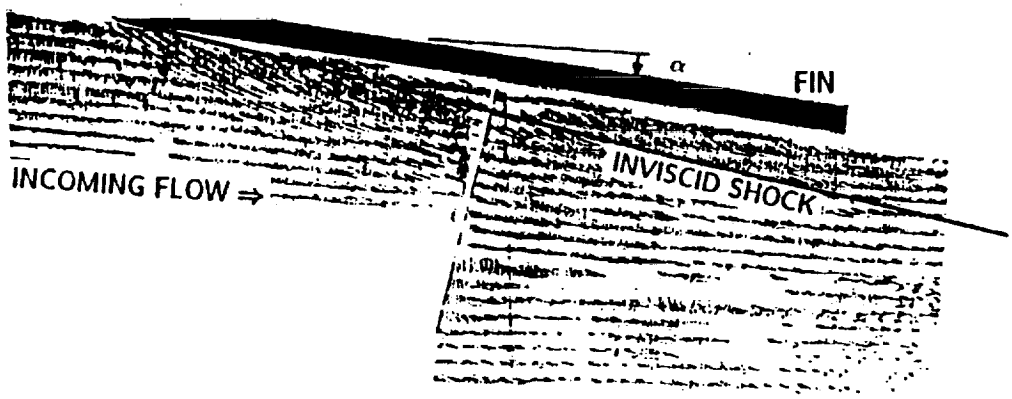

Figure 8: Oil-dot visualization pattern of fin interactions, $\alpha = 5°$.

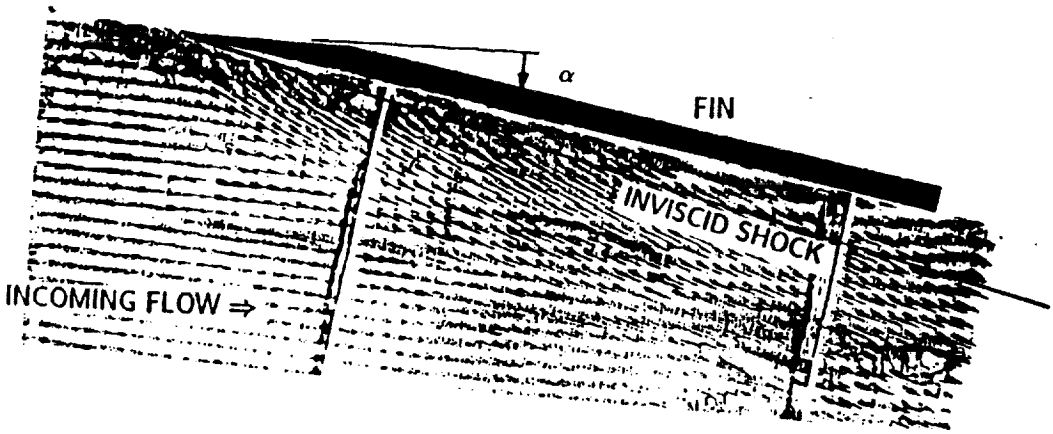

Figure 9: Oil-dot visualization pattern of fin interactions, $\alpha = 10°$.

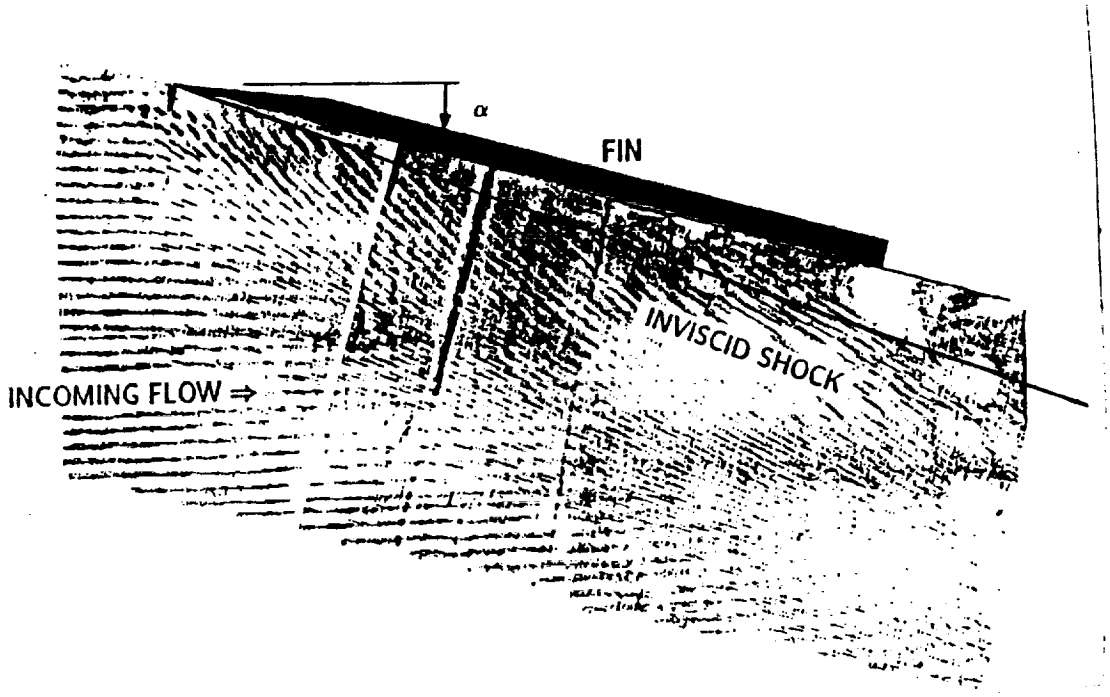

Figure 10: Oil-dot visualization pattern of fin interactions, $\alpha = 15°$.

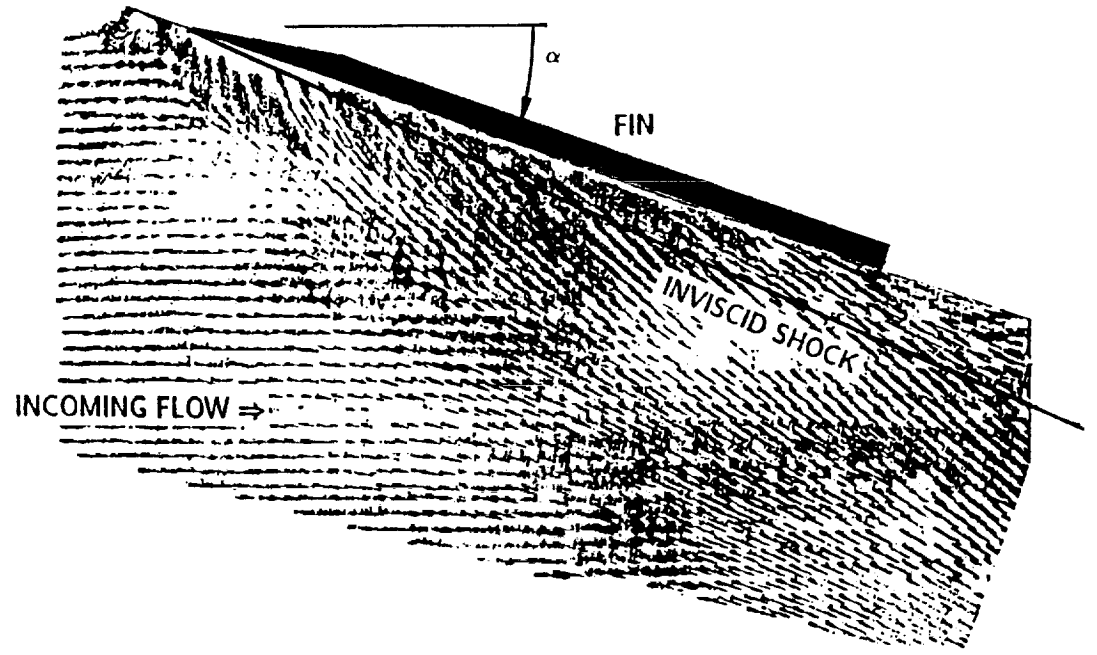

Figure 11: Oil-dot visualization pattern of fin interactions, $\alpha = 20°$.

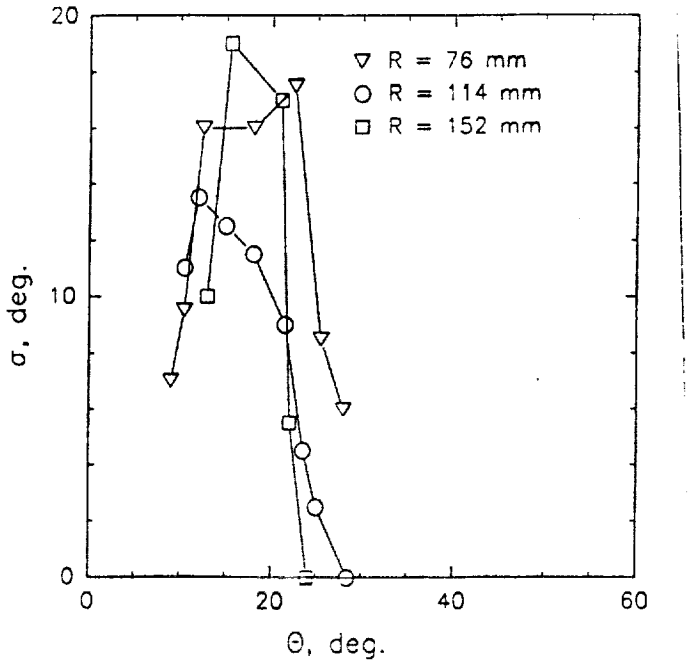

Figure 12: Surface flow deflection angle of fin interactions, $\alpha = 5°$.

pattern with a pronounced curve in the inception region. The curvature, coupled with the relatively poor quality of this trace, made it difficult to determine if the pattern exhibited quasi-conical symmetry. Near the corner with the fin where flow attachment occurred, the dots appeared to be smeared, indicating that the attachment may be unsteady. The patterns due to the $\alpha = 10$, 15° and 20° fins were qualitatively similar to that due to the 5° fin; the major difference was that the extent of the interaction increased. In addition, the streaks were highly deflected and the interaction did not appear to reach a quasi-conical state within the measurement region.

The surface flow deflection angle σ was determined quantitatively from the oil-dot traces and plotted against θ in Figs. 12–15 at three different radii of 76 mm (3 in.), 114 mm (4.5 in.) and 152 mm (6 in.) from the fin apex. The streaks deflected to angles as large as 20° for the $\alpha = 5°$ interaction and deflected to about 40° for the strongest interactions studied. For the strongest interactions, the streak deflections showed local minima which are associated with secondary separation.[19] These dips in the flow deflection angles indicated a convergence of the oil streaks which may not be immediately obvious from visual inspection of the patterns. The present data were consistent with Zheltovodov's secondary separation criterion formulated from supersonic interactions.[6] Also, the patterns showed that σ very near the fin was from 5 to 20° greater than the fin angle. These large deflections suggested that the flow attached very near, if not at, the base of the fin.

Turning next to the surface pressure distribution, these are plotted in Figs. 16–19. The characteristic dip in the pressure distribution in well-separated, supersonic interactions[6] is not seen in the figures even though the interactions are deemed separated from surface visualization. Only in the $\alpha = 20°$ case was there a distinct dip.

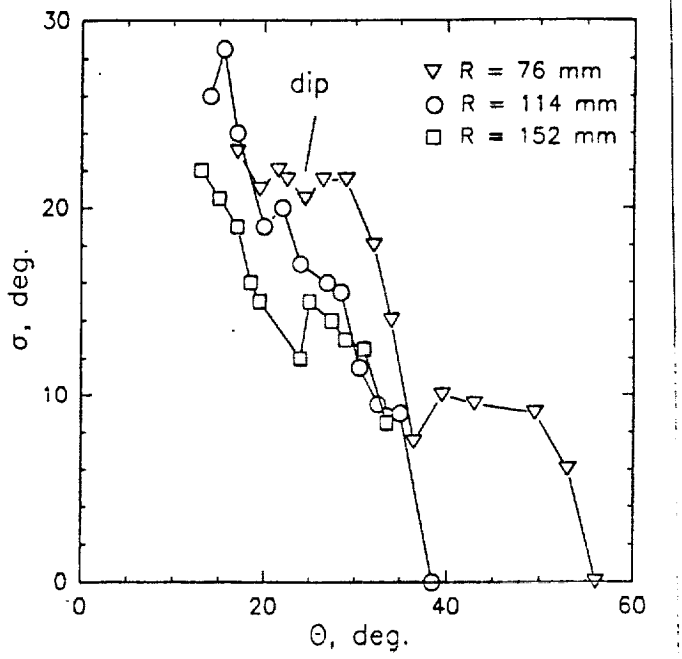

Figure 13: Surface flow deflection angle of fin interactions, $\alpha = 10°$.

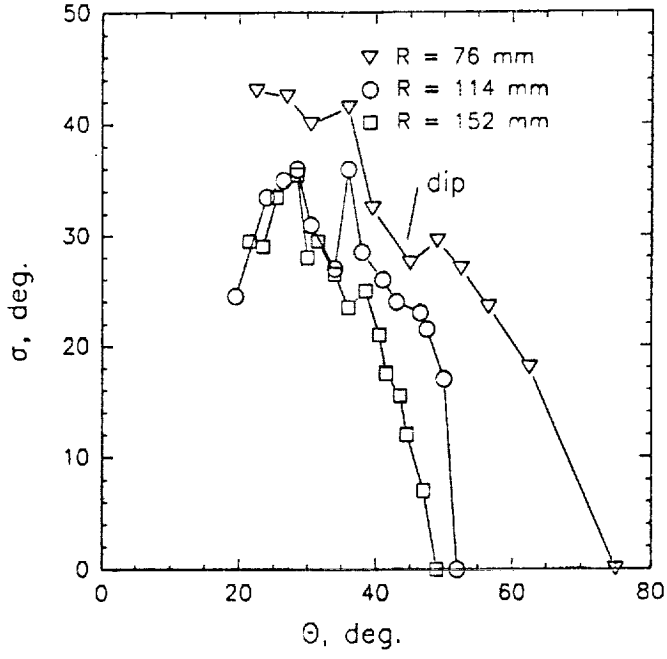

Figure 14: Surface flow deflection angle of fin interactions, $\alpha = 15°$.

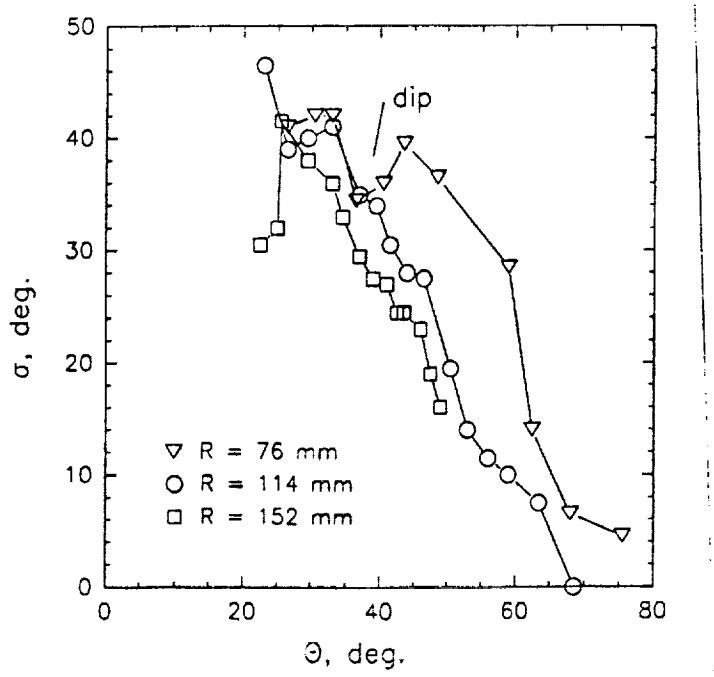

Figure 15: Surface flow deflection angle of fin interactions, $\alpha = 20°$.

There are some possible reasons for the pressure distributions in the present study not possessing a dip. The first is that the interaction is not fully developed, the experiments not being performed far enough from the fin apex to capture a dip. Secondly, the Reynolds number may be lower than those in the supersonic experiments, thereby causing the anomalous result. Thirdly, the reason may be that there are distinct differences between hypersonic and supersonic interactions. Further study at other high Mach numbers and with a longer interaction extent may provide answers.

In general, the surface pressure distributions appeared to take on an approximately bi-level form throughout the interaction. From the upstream influence to near the inviscid shock trace, the surface pressure distributions appeared to be in the form of a "plateau" with $p/p_\infty \approx 2$. This plateau region was fairly large in angular extent, being 20–30° at $r = 114\,\text{mm}$. At the vicinity of the inviscid shock, the pressure began rising rapidly. The subsequent region of high pressure was extremely narrow compared to the plateau region, being only about 5° in angular extent. Except for the weakest case, the surface pressure did not approach the inviscid downstream value, even though the 4° angular spacing of the surface pressure was thought to be able to resolve some detail. This behavior was unlike that found in supersonic interactions where a pressure "overshoot" is found in the farfield of highly-separated interactions.[6] The reason for the observed hypersonic behavior is still not clear at present although it is probably tied to the nature of the impinging jet structure in the extremely congested region near attachment.[43]

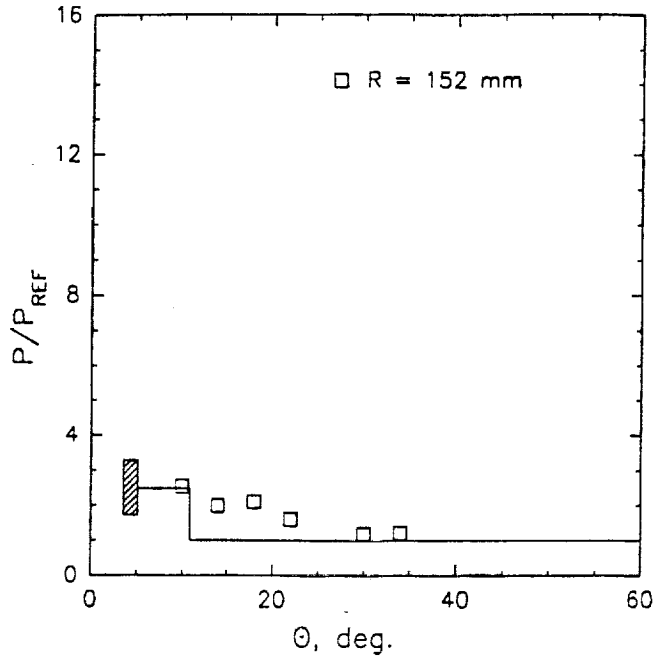

Figure 16: Surface pressure distribution of fin interactions, $\alpha = 5°$.

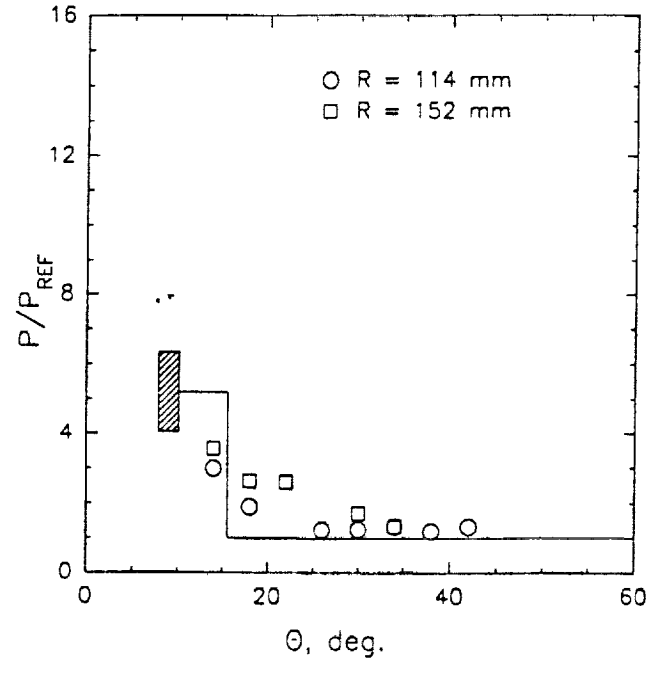

Figure 17: Surface pressure distribution of fin interactions, $\alpha = 10°$.

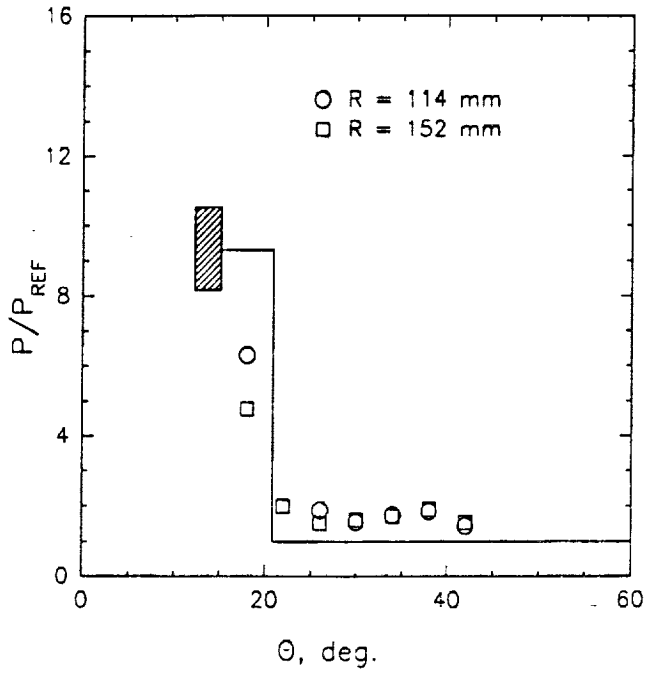

Figure 18: Surface pressure distribution of fin interactions, $\alpha = 15°$.

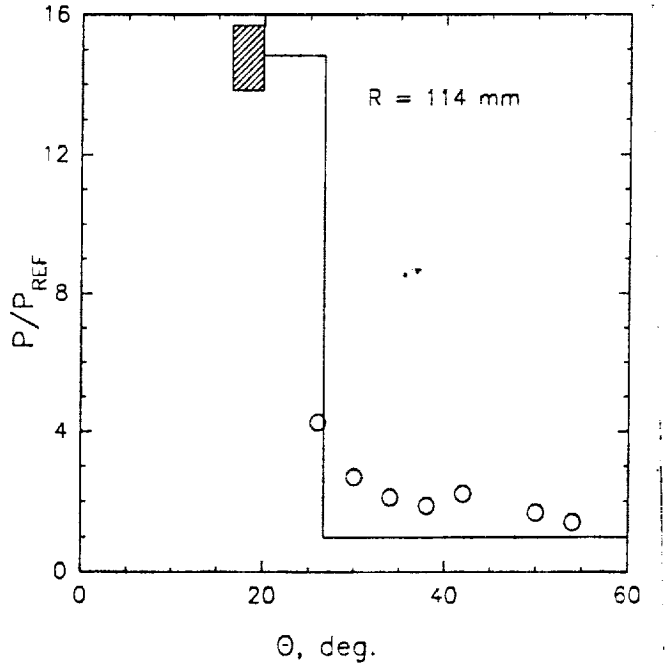

Figure 19: Surface pressure distribution of fin interactions, $\alpha = 20°$.

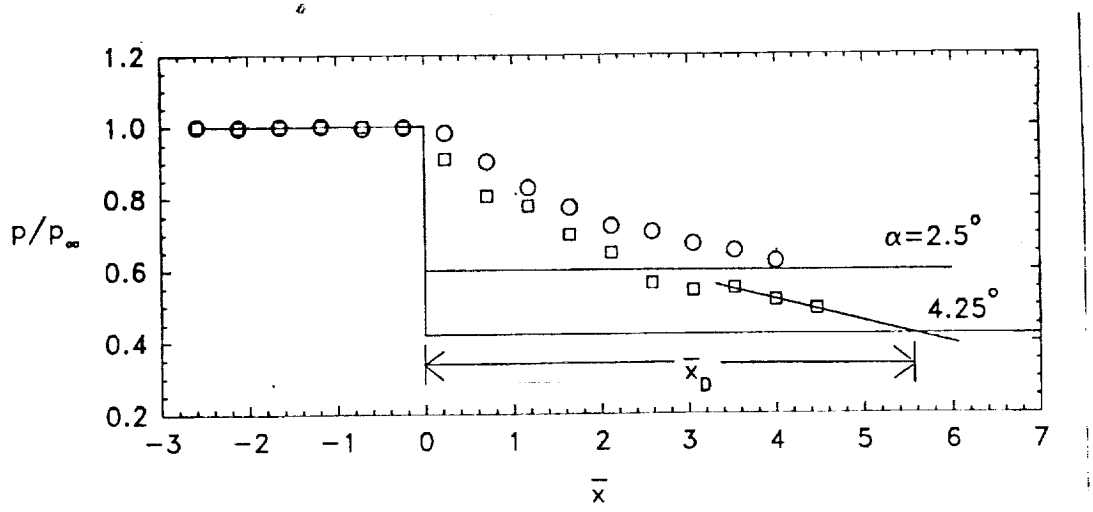

Figure 20: Surface pressure distribution of expansion corners, $\alpha = 2.5$ and 4.25°.

3.2 Expansion Corner Flows

The mean surface pressure distributions for $\alpha = 2.5°$ and 4.25° expansion corners, normalized by the static pressure measured $2.6\delta_o$ upstream of the corner, are plotted in Fig. 20. Also shown are the inviscid pressure distributions for an incoming Mach 8 flow. No upstream influence of the corner was detected, an observation consistent with previous turbulent studies.[31–33] and unlike laminar flows.[44,45] The measured pressures approached the downstream inviscid values some distance $\bar{x}_D \equiv x_D/\delta_o$ from the corners although adequate downstream data could not be obtained due to model limitations. (The pressure decay should strictly be asymptotic to the downstream inviscid value.) The "downstream influence" of the corner $\bar{x}_D$ was estimated as that from the corner to the intersection of the tangent through the downstream pressure distribution with the inviscid downstream pressure as depicted in Fig. 20. The present data showed that the larger the corner angle, the stronger the expansion and thus the longer the downstream influence.

As mentioned previously, it was thought that the the expansion process and the downstream influence may depend primarily on K. Therefore, the downstream influence data are plotted together with data extracted from previous investigations in Fig. 21. Bloy's data[30] show excessive scatter and are included simply to reveal the trend of $\bar{x}_D$ with higher values of K. The collapse of data from Mach 1.76 through 8 supports the validity of K as a scaling parameter, at least for x_D up to $K \approx 1$ where reliable data exist. This validity is particularly striking between the fairly good collapse of Dussauge and Gaviglio's[33] downstream influence with one of the present test cases for approximately the same value of K. Fig. 21 shows that the surface pressure of weak expansions reaches the downstream inviscid value quickly. These weak

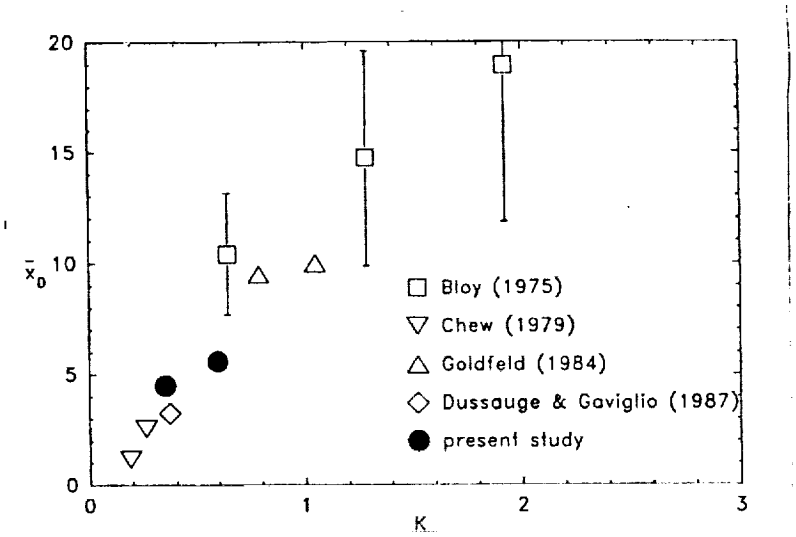

Figure 21: Downstream influence of turbulent flow past expansion corners.

conditions can be achieved at low supersonic Mach numbers even for considerably large corner angles as in the case of Dussauge and Gaviglio.[33] In the past, this rapid pressure decay led to the conclusion that the surface pressure reaches the downstream inviscid value in a distance of about one incoming boundary layer thickness.[46]

The effect of the expansion on surface pressure fluctuations was also examined. Previous studies[33,47] applied rapid distortion approximations to predict the Reynolds stresses with good accuracy. Both experiment and analysis show dramatic decreases in velocity fluctuations and Reynolds stresses but not of the mass-flux fluctuations.[47] Further, mean velocity profiles[32,33] show tremendous amounts of distortion of the outer layer from the fully developed, equilibrium, turbulent profile. In addition, in some instances a "sub-boundary layer" develops through a thickening of the viscous sublayer which indicates that the boundary layer may "relaminarize,"[46] a term which should however be used with caution in view of the nearly unattenuated mass-flux fluctuations downstream.[47]

The pressure fluctuations remained Gaussian downstream of the expansion corner as is illustrated in Fig. 22 which plots the normalized probability density function (pdf) against the standard deviation from the mean[48] for an undisturbed location at $\bar{x} = -0.71$ and for downstream locations at $\bar{x} = 1.18$. The pdf of the 4.25°expansion showed more distortion from the Gaussian than that of the 2.5° expansion. This might be due to an insufficiently long data record because contamination from the tunnel starting and stopping processes gave rise to slightly higher pressures at both ends of the data record, thereby causing the pdf to be skewed slightly.

The standard deviations of the surface pressure fluctuations were normalized by the local mean surface pressure, by the dynamic freestream pressure at $\bar{x} = 0$ and

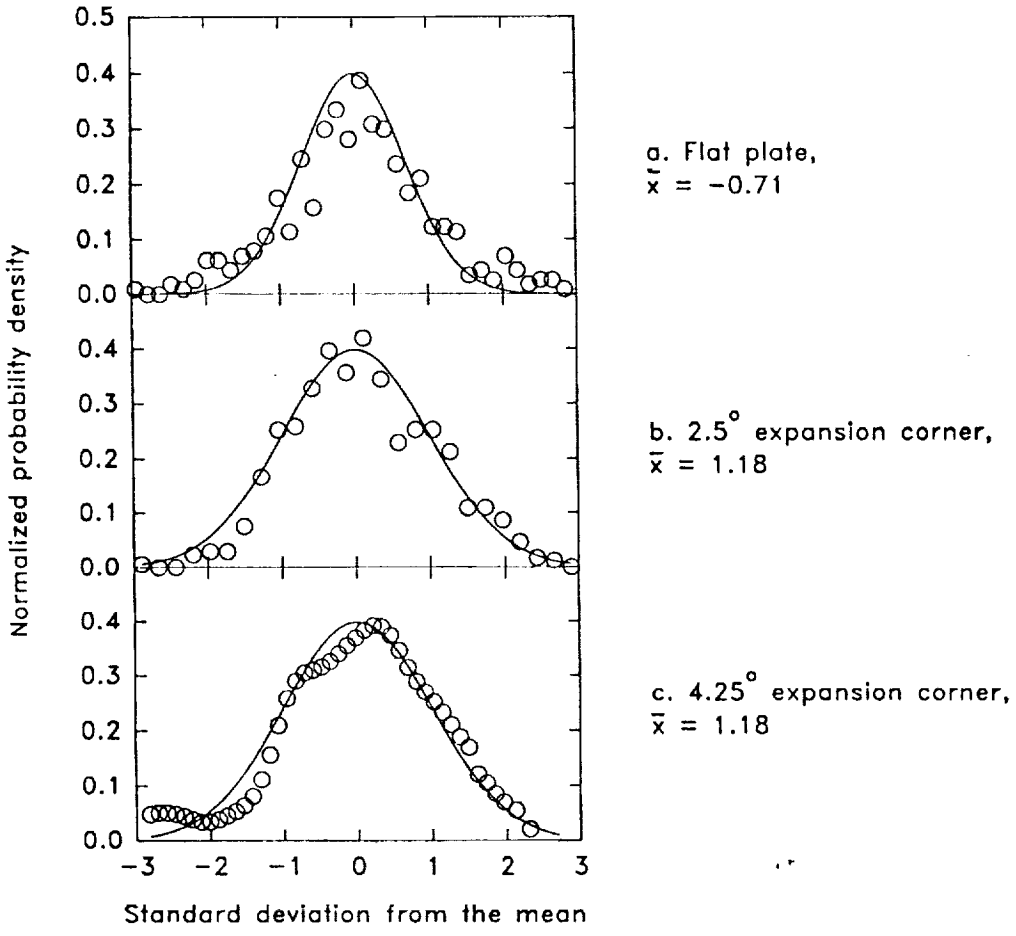

Figure 22: PDFs of surface pressure fluctuations. a. Flat plate. b. $\alpha = 2.5°$. c. $\alpha = 4.25°$.

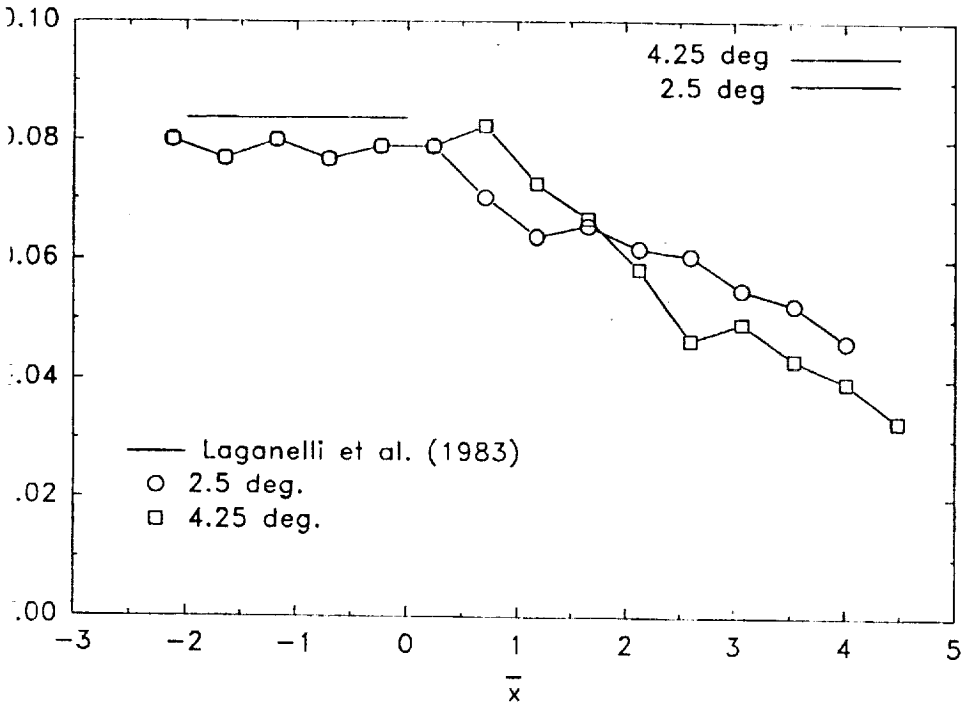

23: Standard deviation of surface pressure fluctuations past expansion corners
ized by local mean pressure.

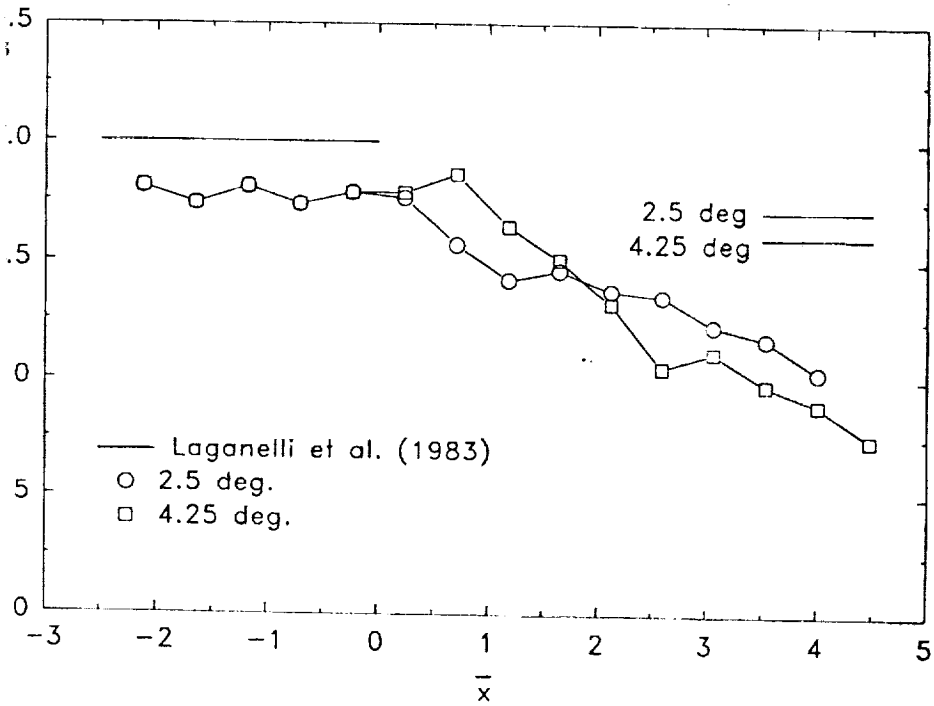

1: Standard deviation of surface pressure fluctuations past expansion corners
ed by incoming freestream dynamic pressure.

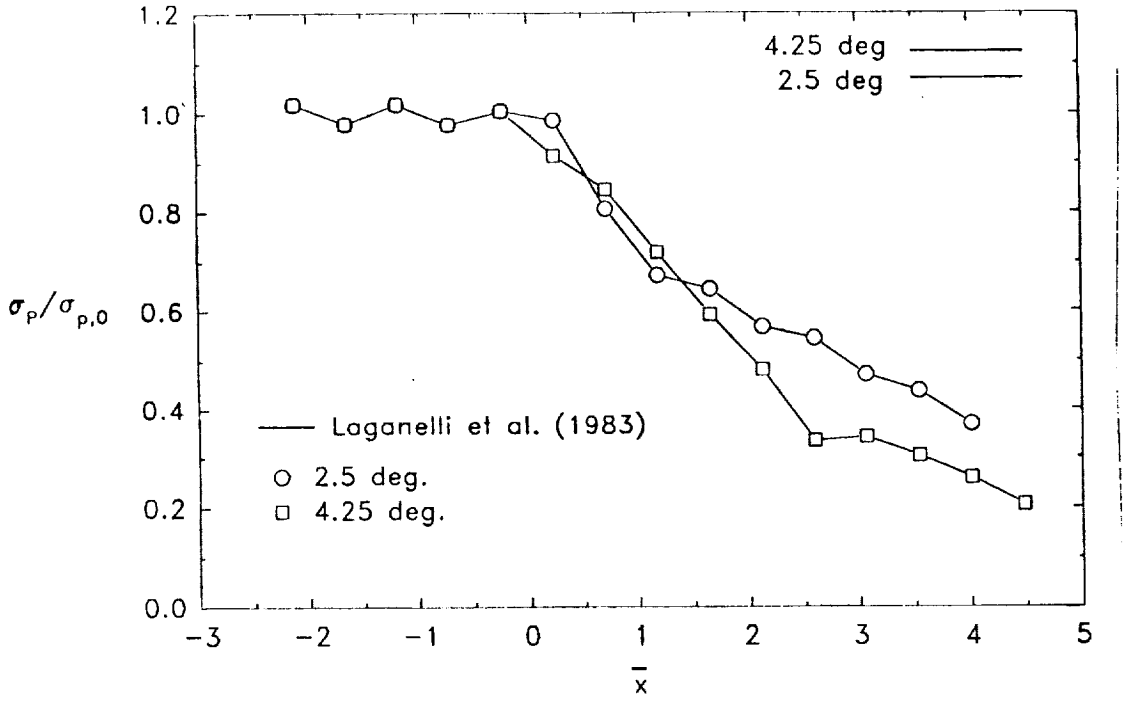

Figure 25: Standard deviation of surface pressure fluctuations past expansion corners normalized by incoming value.

by the incoming standard deviation, and are plotted in Figs. 23–25 respectively. The ensemble of σ_p data upstream of the corner had an rms error band of about ± 2 percent, which was presumed to be the error in the σ_p estimate through the expansion downstream as well. Plotted in Fig. 23 for $\bar{x} < 0$ is Laganelli et al.'s[49] semi-empirical correlation for a flat-plate flow. The present measurements upstream of the corner were slightly below, but probably within the range of validity, of that predicted by Laganelli et al. The lower fluctuation level measured might be due to the limited frequency bandwith of the present experiments. Nonetheless, the discrepancy between the present data and Laganelli et al.'s prediction was not severe.

In addition, the data showed the intuitive expectation of a decrease in the fluctuations downstream of the expansion corner, with σ_p/p decreasing from about 0.08 upstream to about 0.046 and about 0.033 for $\alpha = 2.5$ and 4.25° respectively at $\bar{x} = 4$. Similarly, $\sigma_p/q_{0,\infty}$ decreased from about 0.002 on the flat plate to about 0.001 and about 0.000 7 for the two respective corners at $\bar{x} = 4$, Fig. 24. Moreover, the σ_p data did not show any asymptotic behavior or an increase within the measurement range that might indicate either formation of a new "quiescent" sub-boundary layer or retransition to a fully-developed turbulent flow. The data indicated that the effect of the expansion process on the surface pressure fluctuations was incomplete even at the most downstream measurement station and, most likely, that the boundary layer was not in equilibrium. Further, using the predictions of Laganelli et al.,[49] the downstream pressure fluctuations for a fully developed, turbulent, flat plate flow were estimated and are shown as short horizontal lines at the right in Figs. 23–25. Fig. 23 shows that at the most downstream measurement station, σ_p/p was about 45 percent

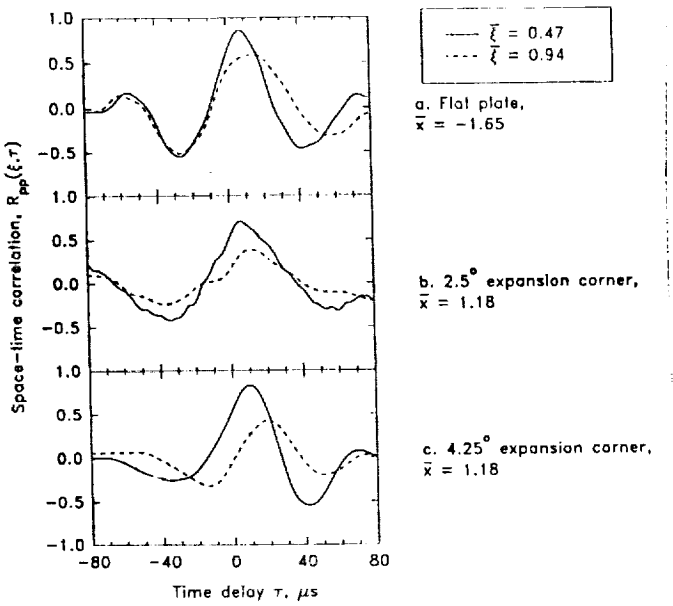

Figure 26: Space-time correlations of surface pressure fluctuations past expansion corners. a. Flat plate. b. $\alpha = 2.5°$. c. $\alpha = 4.25°$.

and about 60 percent below the turbulence predictions for the two respective weaker and stronger expansions. In terms of dynamic pressure, the surface pressure fluctuations were about 40 percent below the turbulent predictions for the 2.5° corner and was about 53 percent below the predictions for the 4.25° corner, Fig. 24. It is obvious that the surface pressure fluctuations for the stronger expansion would take a longer distance to recover to the presumably ultimate turbulent level given a sufficiently long downstream length.

Another way of viewing the surface pressure fluctuation development is to compare the fluctuations with that of the incoming boundary layer, Fig. 25. Fig. 25 emphasizes even more clearly the attenuation provoked by the favorable pressure gradient. The surface pressure fluctuations four boundary layer thicknesses downstream of the corner damped to 37 percent and 21 percent of the incoming value for the 2.5° and 4.25° corners respectively. Possibly, these downstream fluctuation levels could be the "tare" levels of the shock tunnel although this was expected to be unlikely since the tunnel vibrations were at lower frequencies. The data indicated once again that the flow at four to five boundary layer thicknesses downstream of the corner was still relatively quiescent. Although data were unavailable presently and are probably unfeasible to obtain, it is thought that the boundary layer would revert to an equilibrium turbulent state and that the entire "recovery" process would occupy a long distance of possibly hundreds of boundary layer thicknesses downstream of the corner.[50] This behavior can be significant in designing high-speed vehicles where even relatively weak expansions such as studied presently can be used to severely attenuate surface pressure fluctuations perhaps for considerable distances downstream.

The space-time cross correlation of the surface pressure fluctuations were examined as well. Three space-time correlations are plotted in Figs. 26*a–c*, namely those of a flat plate and the two expansion corners. That of the flat plate was obtained upstream of the corner for transducer spacings of $\xi = 0.47\,\delta_o$ and $0.94\,\delta_o$ whereas those of the expansions were obtained with the first transducer located at $x = 1.18\,\delta_o$ and with two additional transducers downstream spaced at $0.47\,\delta_o$ intervals. The cross correlations downstream of the expansion appeared broadly similar in shape as that of the flat plate. These cross correlations were also typical of turbulent flows in which the maxima occur at a positive time delay, τ^*. A convection velocity can therefore be defined as

$$U_c \equiv \xi/\tau^*. \tag{3}$$

The convective velocity suggests that a disturbance, in this case a wall pressure signal, is convected from one transducer to a downstream transducer at a time interval τ^*. The actual estimates of U_c in the present experiments were prone to error due to difficulties in resolving the maxima accurately. A one μs error resulted in an error of ten percent to U_c; similar error bands can be inferred from previous investigations.[17] Within measurement accuracy, U_c for a given transducer was roughly constant regardless of the test configuration. Thus, with $\xi = 0.47\,\delta_o$, $U_c/U_\infty = 0.65$, 0.71 and 0.55 for the flat plate, and for the 2.5° and 4.25° corner respectively, where U_∞ was the incoming freestream velocity. Further, with $\xi = 0.94\,\delta_o$, $U_c/U_\infty = 0.70$, 0.79 and 0.60 for the three configurations respectively. There appeared to be a definite trend of an increase of U_c with ξ, this being also observed by previous investigators for flat plate flows.[17]

The increase in convection velocity is commonly interpreted as follows. Small scale (or high frequency) components of the pressure fluctuations are thought to travel downstream slowly since these fluctuations, being small, would be convected at velocities more typical of the lower portion of the boundary layer. These small fluctuations also have a short "time constant" and decay rapidly. On the other hand, the large-scale pressure fluctuations can be expected to be associated with large eddies within the boundary layer which are convected downstream at higher velocities.

The individual transducer data were correlated by themselves to give rise to autocorrelations $R_{pp}(\tau)$. Although autocorrelations are commonly plotted with the time delay τ on the abscissa, the present data are plotted against a nondimensional "convection distance" $\bar{D}_c = \tau\,U_c/\delta_o$ to facilitate the discussion, where a value of $U_c \approx 0.65\,U_\infty \approx 810\,\mathrm{m\,s^{-1}}$ (2,650 ft/sec) was used. Thus, both U_c and δ_o were assumed constant although they were expected to increase through the expansions. The increase of both terms were approximately compensated by the normalization. Using $\bar{D}_c$ tacitly accepted Taylor's hypothesis, $\bar{D}_c$ representing the distance in terms of δ_o that a disturbance was convected at a velocity U_c. The autocorrelations of the surface pressure fluctuations $R_{pp}(\tau)$ are plotted in Fig. 27 for both corner angles. In the figures, the autocorrelation upstream of the corner is shown as a thick solid line whereas the autocorrelations downstream are shown as symbols connected by dotted

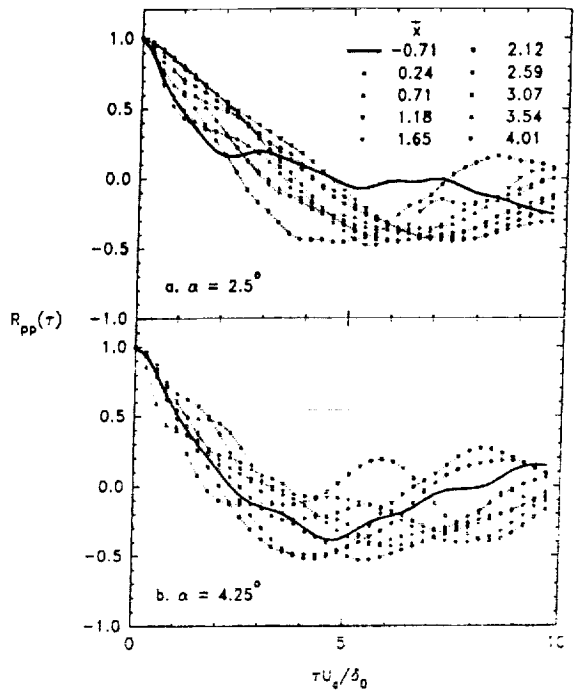

Figure 27: Autocorrelations of surface pressure fluctuations past expansion corners. a. $\alpha = 2.5°$. b. $\alpha = 4.25°$.

lines. The symbols denote only one quarter of the total data for each correlation to avoid cluttering the plots. Also, the legend for Fig. 27b is the same as that for Fig. 27a and is omitted for clarity.

The autocorrelations showed shapes typical of those encountered in surface pressure measurements at lower Mach numbers, namely, they exhibited a rapid decrease followed by a shallow negative lobe and a subsequent shallow positive lobe. For larger values of $\bar{D}_c$, the shallow positive lobe in $R_{pp}(\tau)$ in the present experiments might be affected by disturbances from flow starting or stopping because of the short duration of the quasi-steady test period. It was difficult to detect any trends in the autocorrelations which may be because the expansions were weak.

An integral scale and a microscale were estimated from the autocorrelations. These estimates were of the ensemble of the downstream measurements for each test configuration. The determination was affected by "jitters" and "bumps" in the curves. The integral scale, found by integrating the autocorrelations, was estimated to be about $4.5\,\delta_o$ for the 2.5° expansion and about $6.7\,\delta_o$ for the 4.25° expansion, with an rms scatter of ± 20 and ± 10 percent. (In physical dimensions, the integral scales were $75 \pm 15\,\mu$s and $110 \pm 10\,\mu$s respectively.) The integral scale obtained was larger than the incoming boundary layer thickness, a phenomenon also found in previous flat-plate studies which was attributed by Dolling and Dussauge[17] to the limited data bandwidth. Despite the difficulties associated with data bandwidth, the integral scale is a rough measure of the interval that a turbulent signal is correlated with itself, and the trend of the data indicated that the "large-scale" surface pressure fluctuations maintained their identities longer for the stronger expansion.

The microscale determination was also affected by the "jaggedness" of the auto-

correlations, perhaps more so than for the integral scale, and the following technique was used for its estimation. Only data very near the origin were fitted to an osculating parabola, with data thresholds of $\tau U_c/\delta_o = \pm 2, \pm 1, \pm 0.75, \pm 0.5$, and ± 0.25. A second-order least-squares fit was then performed on the microscales obtained from the data within the five individual thresholds. Extrapolation to $\tau U_c/\delta_o \rightarrow 0$ of the curvefit constants obtained for the data thresholds then gave the desired value of the microscale. The composite value of the microscale for both expansion corners given by the above technique was about $\tau U_c/\delta_o = 1$, with an rms scatter of 20–40 percent. This value was also on the same order as that found for the upstream flow. In physical dimensions, this corresponded to a time of 16 μs and, invoking Taylor's hypothesis, a distance of about one boundary layer thickness. The present estimates were much lower than those of Raman[51] for a Mach 7.4 flow past a flat plate in which the microscale was about 50 μs, and were thought to be more accurate since only data very near the origin were fitted to the osculating parabola by a limiting process.

3.3 Shock Impingement on a Flat Plate

To ultimately understand the mutual interaction between an impinging shock wave and an expansion corner, preliminary experiments were performed of a shock impinging on a flat plate. A weak shock impinged the flat plate at 0.77 m (30.25 in.) from the leading edge and induced an unseparated interaction. The unseparated nature of the interaction can be deduced from previous correlations[4] or inferred from the surface pressure distributions in which no plateau or dip, which indicates separation, was seen, Fig. 28. In Fig. 28, the streamwise location is referred to the inviscid shock impingement position on the flat plate.

The size of the interaction, based on the mean surface pressure distribution, was larger for the stronger shock, it being about $5.5\delta_o$ compared to about $2\delta_o$ for the weaker case. (The slight irregularity of the downstream surface pressure for the 2° shock generator may be due to small deviations in setting the angle between runs.) From the surface pressure distribution, an upstream influence scale was obtained.[6] The upstream influence x_u was normalized by the incoming boundary-layer momentum thickness δ_o^* and plotted against the inviscid pressure ratio p_F/p_1 in Fig. 29. The lack of detailed, hypersonic, upstream influence data prompted a comparison with some Mach 3 data instead. For attached flows at Mach 8 and 3, the normalized, upstream influence are approximately the same. However, the present unseparated case had a smaller upstream influence than separated flows at Mach 3 when $p_F/p_1 > 4$.[52]

The unsteadiness of the interaction was also explored by an examination of the surface pressure fluctuations. Figs. 30*a–c* plot the standard deviations of the pressure fluctuations σ_p normalized by the local mean pressure p_w, the upstream rms pressure $\sigma_{p,o}$ and the upstream dynamic pressure q_∞ respectively. The general characteristics of the rms distribution were typical of some previous supersonic studies.[54–56] Fig. 30*a* shows that the intensity of the surface pressure fluctuations σ_p/p_w increased rapidly

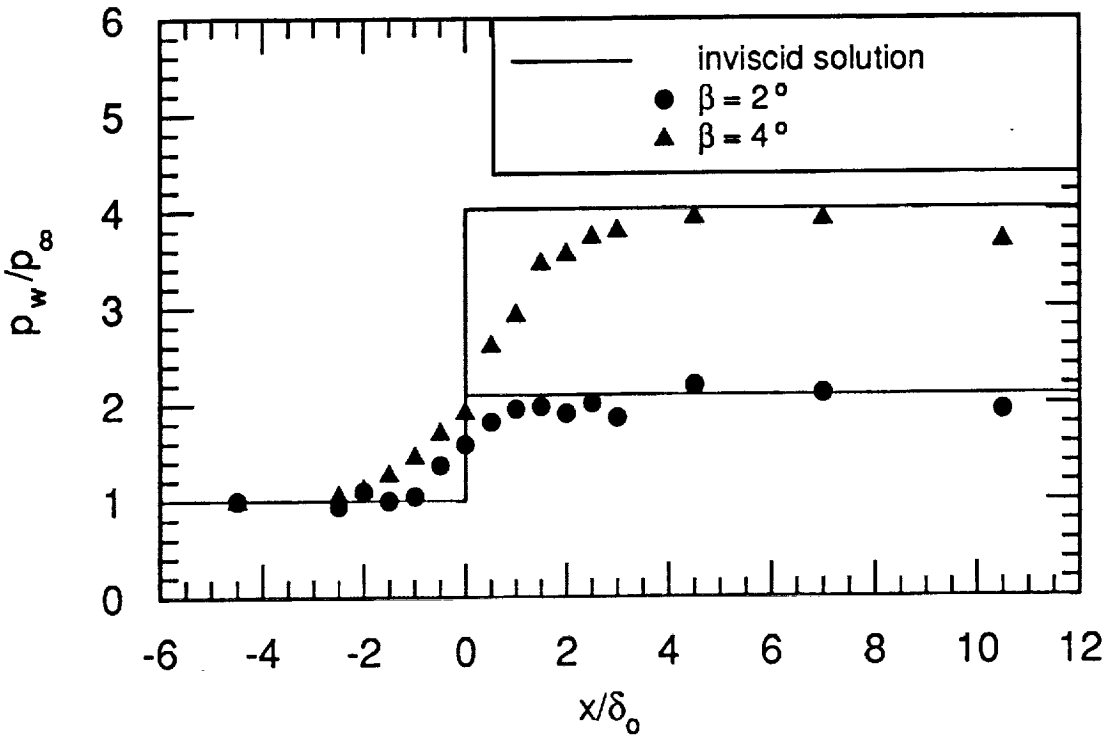

Figure 28: Surface pressure distributions of shock impingement on flat plate, $\beta = 2°$ and 4°.

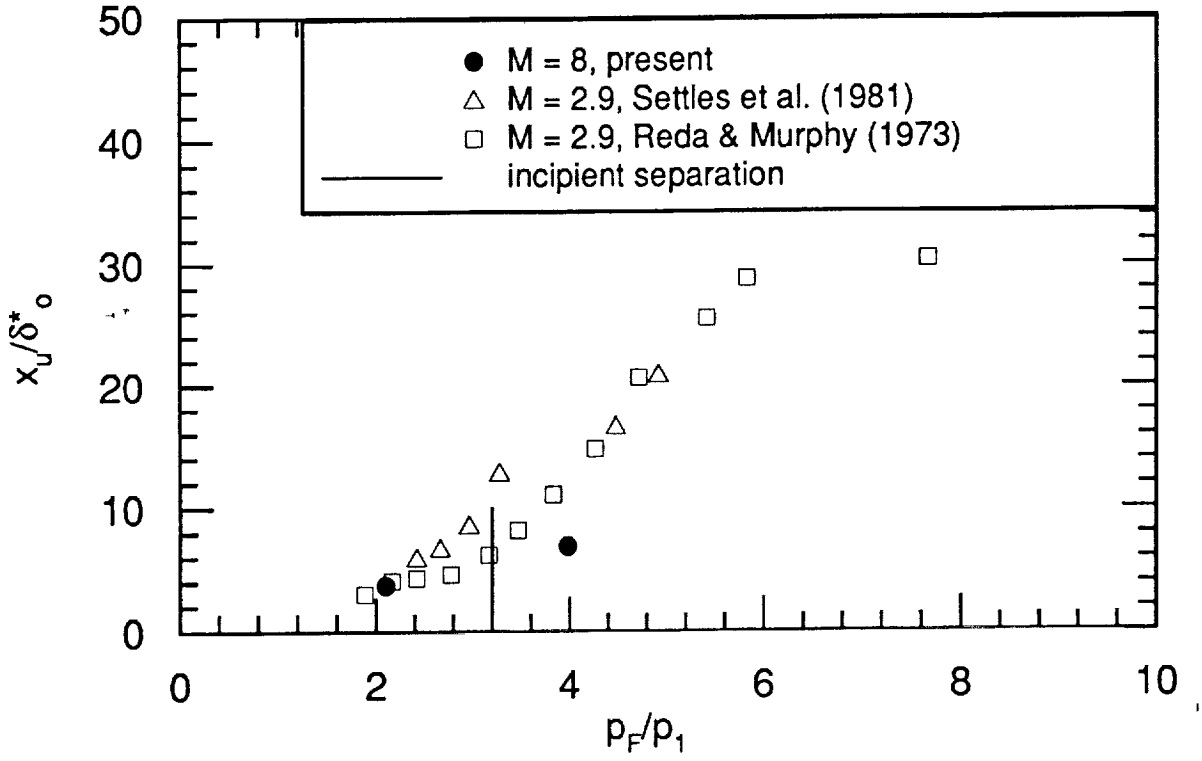

Figure 29: Upstream influence of shock impingement on flat plate.

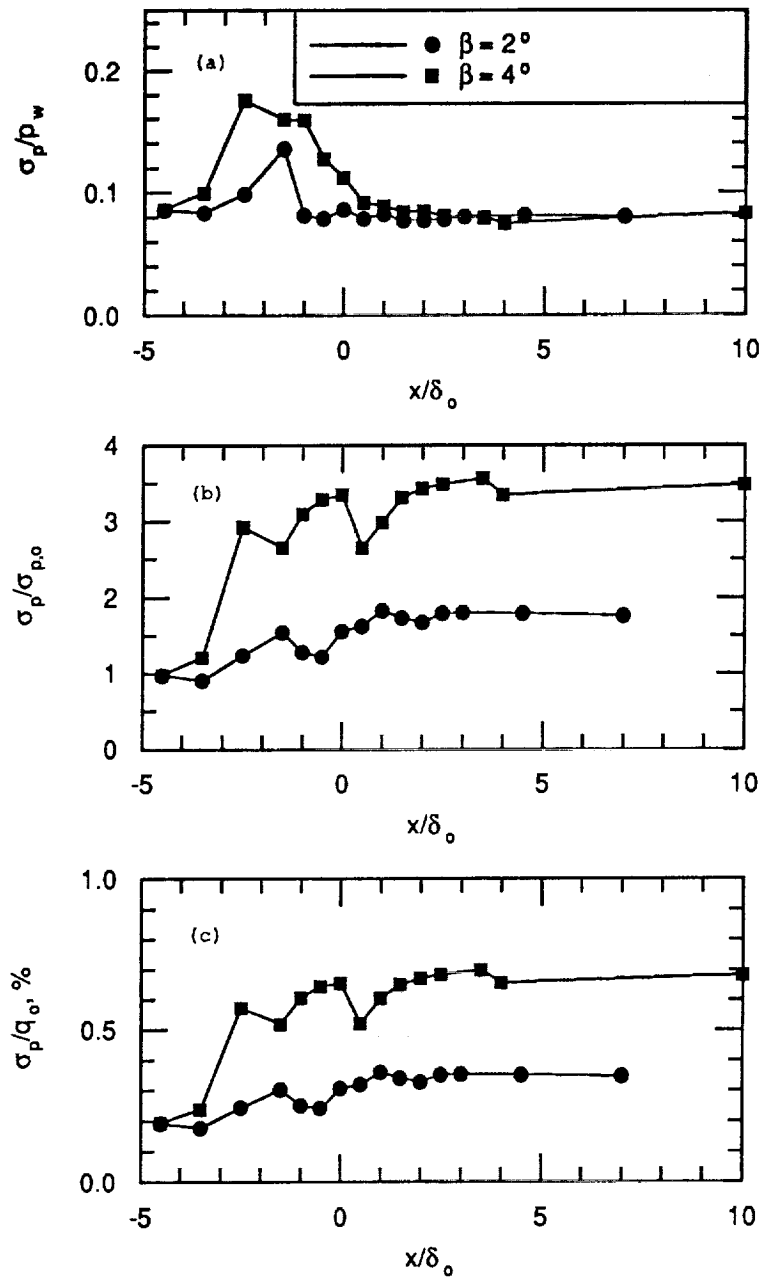

Figure 30: Standard deviation of surface pressure fluctuations due to shock impingement on a flat plate.

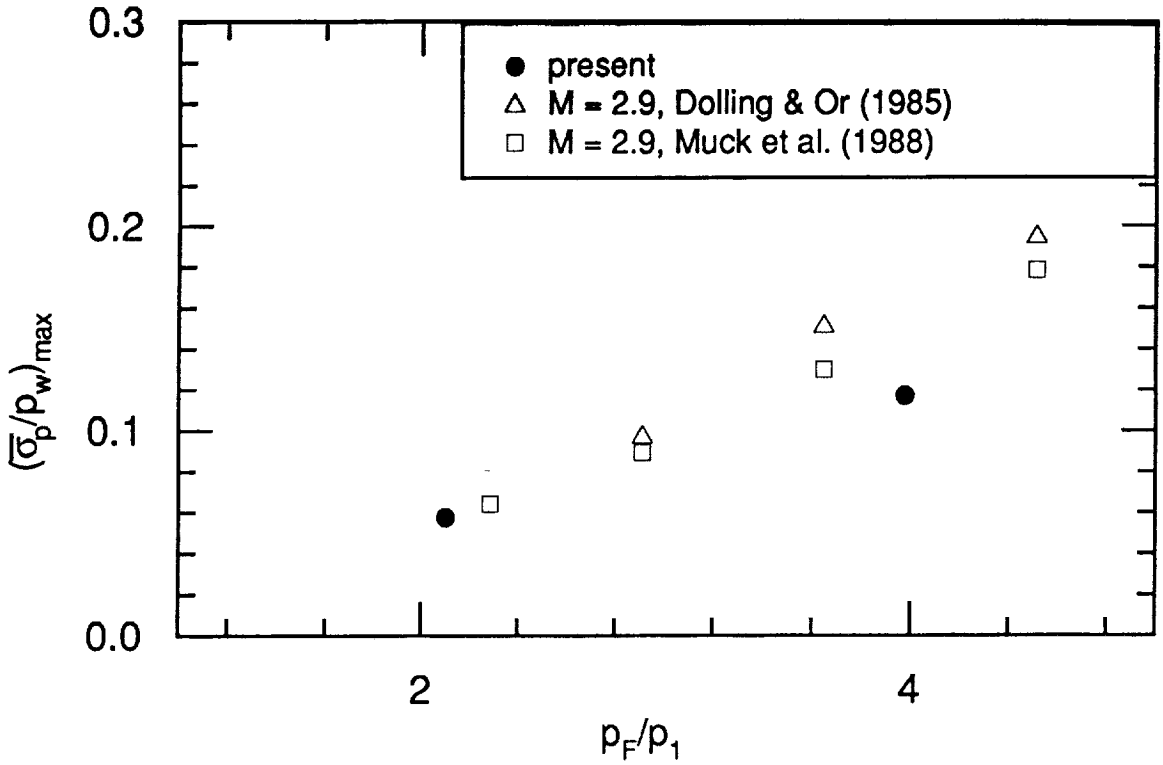

Figure 31: Maximum pressure fluctuation due to shock impingement on a flat plate.

downstream of the upstream influence, reached a maximum and then decreased gradually to the level of the undisturbed, flat plate value. The undisturbed rms level was reached in about 2-3δ_o downstream of the inviscid shock impingement position. The data also showed the effect of shock strength in which the maximum rms value was larger for the stronger interaction. Moreover, the extent of the disturbance as determined by the rms pressure distribution was larger for the stronger interaction. Figs. 30*b*,*c* emphasize the unsteadiness, in which the rms pressure fluctuations increased at the start of the interaction and reached a plateau. In particular, the plateau in Fig. 30*c* was about 0.3 and 0.7 percent of q_∞ due to the 2° and 4° deflections whereas σ_p of the incoming flow was only about 0.2 percent of q_∞. Obviously, even weak shocks are capable of significantly amplifying surface pressure fluctuations in a hypersonic flow. The increase of the surface pressure fluctuations is thought to be due to turbulence amplification.[57]

The peak in the rms pressure fluctuation in Fig. 30*a* is a characteristic of shock wave boundary-layer interactions. In Fig. 31, the normalized peak rms pressure fluctuation $(\bar{\sigma}_p/p_{w,o})_{max}$ is plotted against the shock strength p_F/p_1 and $\bar{\sigma}_p \equiv \sigma_p - \sigma_{p,o}$. The collapse of the present data and previous Mach 3 data[54,56] is fairly good. Tran[57]

suggests that the presence of a peak in the rms pressure fluctuation indicates strong intermittent behavior at start of the interaction. This intermittent nature is further examined through probability density functions which are summarized in Figs. 32 and 33. For the weaker case where $\beta = 2°$, the pdf was slightly skewed negatively at $\bar{x} = -0.5$, with the most probable value at half an rms count below the mean. The other stations upstream or downstream of $\bar{x} = -0.5$ showed random behavior. The pdf of stronger case where $\beta = 4°$ was more skewed near the upstream influence line ($\bar{x} = -2.5$ as determined from the mean surface pressure distribution). For the stronger interaction, the pdf was bimodal further downstream at $\bar{x} = 1.5$. The surface pressure signal alternated between two maxima of the probability curve ($-0.75\sigma_p$ and $0.25\sigma_p$) which is characteristic of intermittent shock motion through the boundary layer. Thus, intermittent behavior existed even in unseparated hypersonic interactions. According to Dolling and Or,[54] the intermittency arises from the wall pressure alternating between that of the undisturbed boundary layer and that of the flow downstream of the shock. Finally, the pdfs near the inviscid shock impingement location was nearly Gaussian with the most probable value slightly above the mean as observed by Dolling and Or.[54]

The mean boundary-layer development was examined through pitot pressure measurements 12.7–38.1 mm (0.5–1.5 in.) downstream of the shock impingement position. The pitot pressure profiles are shown in Fig. 34. Distance and pressure are normalized with respect to the incoming boundary layer thickness and the pitot pressure at the boundary-layer edge. The abscissa is offset for clarity. The normalized pitot pressure profiles showed similiar features as those of previous studies.[58,59] In the present profiles, a "kink" associated with the pressure jump across the reflected shock can be seen near the test surface, from which it can be deduced that the reflected shock was imbedded inside the boundary layer through the measurement region.

3.4 Mutual Interaction Between a Shock and an Expansion Corner

The mutual interaction between an impinging shock wave and an expansion corner in a turbulent boundary layer is discussed here. The interactions generated were weak and in one case, the shock was nearly "cancelled" by the expansion in the sense that the downstream static pressure was approximately equal to that upstream of the interaction. The shocks impinged the flat plate either at the corner or at $\pm\delta_o$ from it. Twelve distinct test cases were examined.

The normalized surface pressure distributions are plotted in Figs. 35–37. In these figures, the pressure distributions for the 2.5° expansion corner are shown on top while those for the 4.25° expansion corner are shown below. In each figure, pressure distributions for the two deflection angles of $\beta = 2°$ and 4° are presented together with the inviscid distribution.

In the absence of the downstream expansion corner, the surface pressure eventually

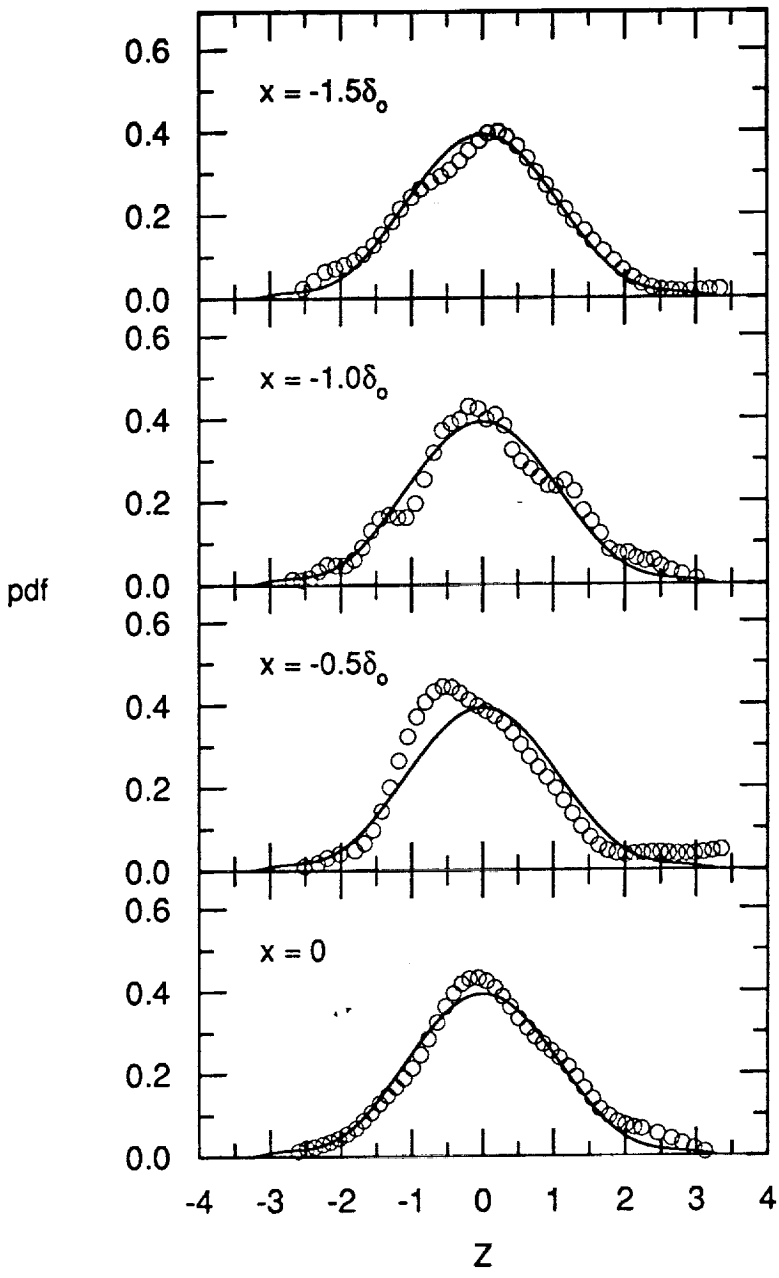

Figure 32: PDFs of shock impingement on flat plate, $\beta = 2°$.

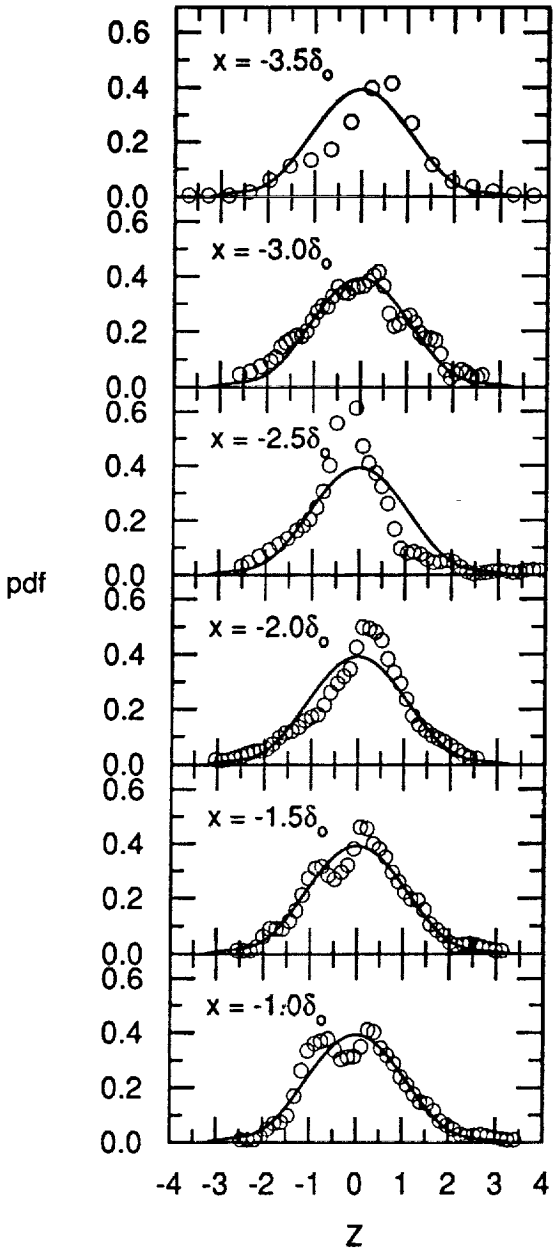

Figure 33: PDFs of shock impingement on flat plate, $\beta = 4°$.

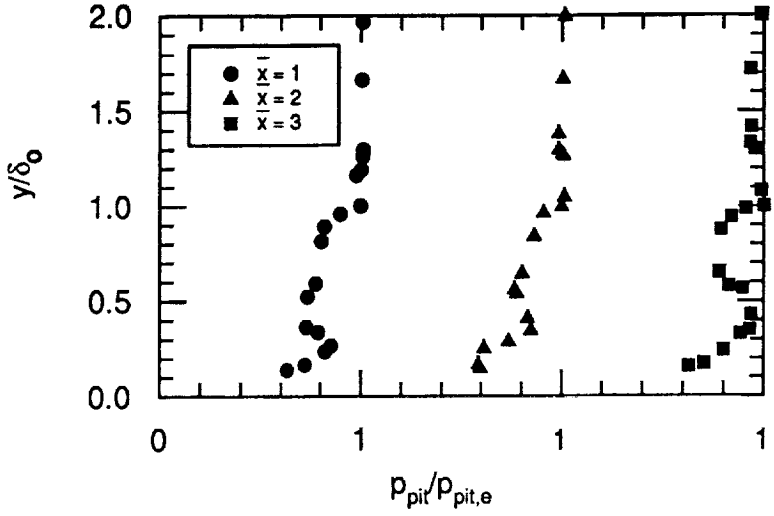

(a) Flat plate, $\beta = 2°$.

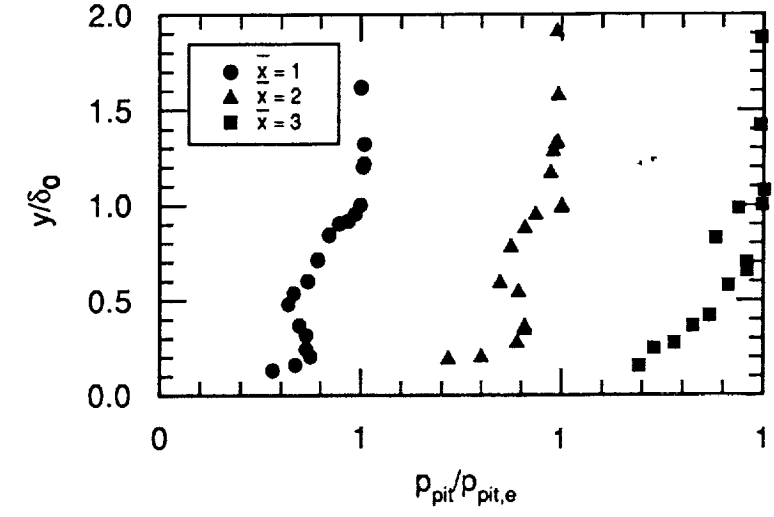

(b) Flat plate, $\beta = 4°$.

Figure 34: Pitot pressure profiles of shock impingement on flat plate, $\beta = 2°$ and $4°$.

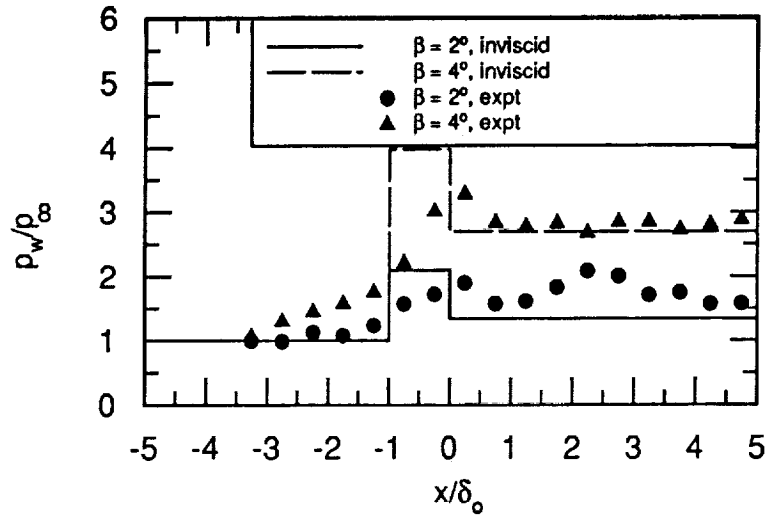

(a) 2.5° expansion corner.

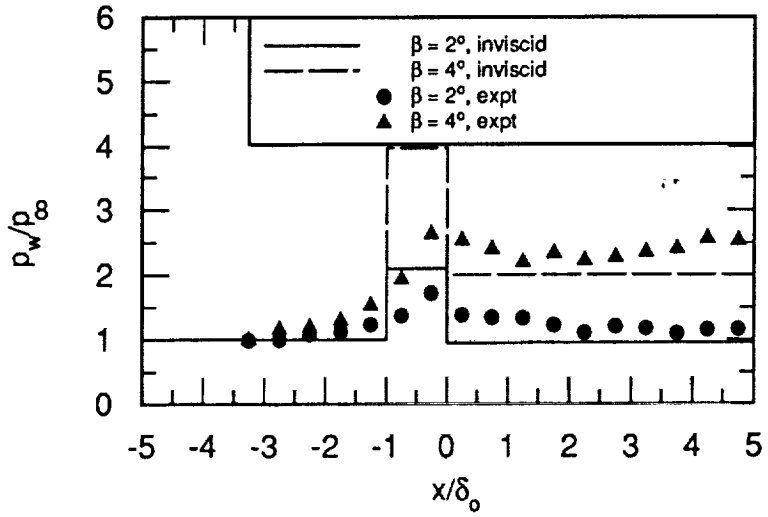

(b) 4° expansion corner.

Figure 35: Surface pressure distributions due to impinging-shock–expansion-corner interaction, $\bar{x}_{sh} = -1$.

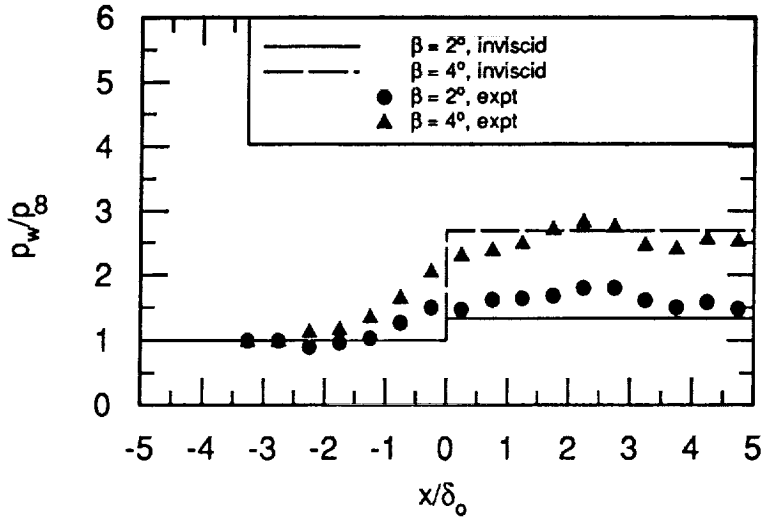

(a) 2.5° expansion corner.

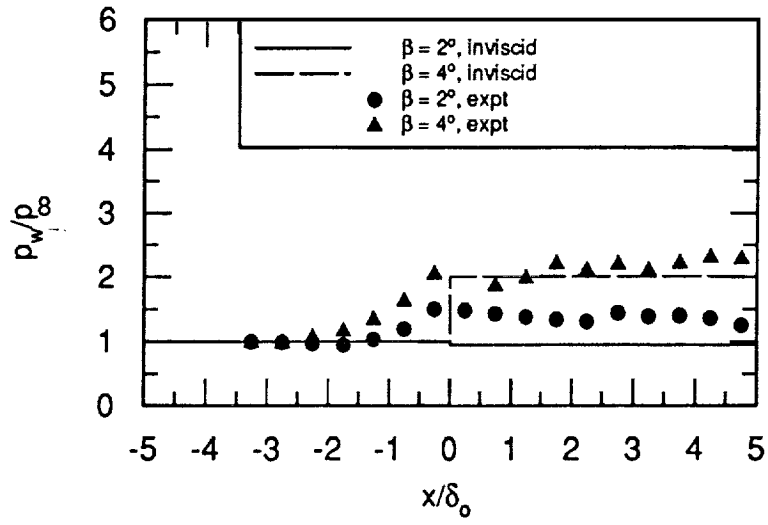

(b) 4.25° expansion corner.

Figure 36: Surface pressure distributions due to impinging-shock–expansion-corner interaction, $\bar{x}_{sh} = 0$.

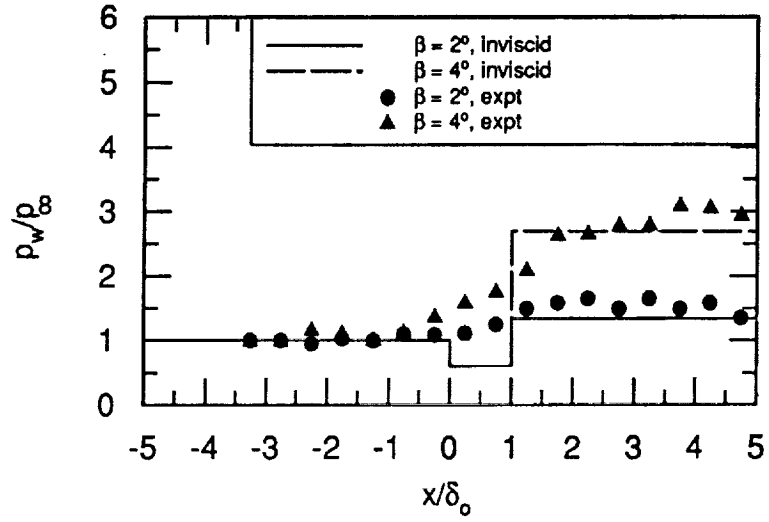

(a) 2.5° expansion corner.

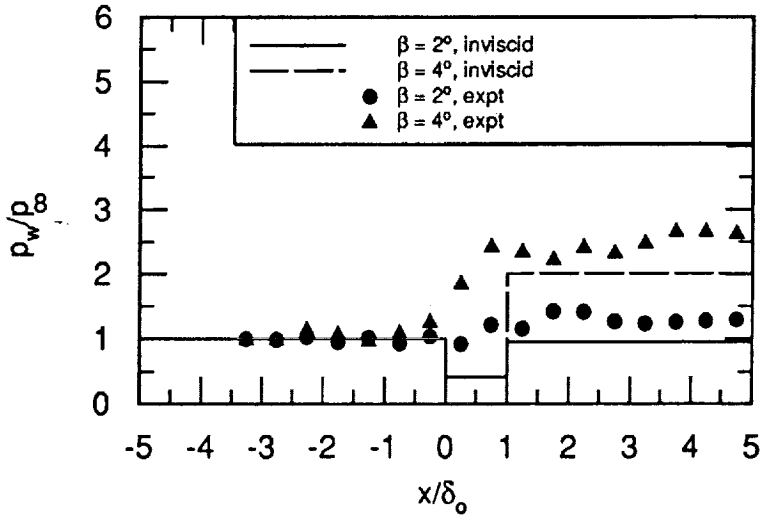

(b) 4.25° expansion corner.

Figure 37: Surface pressure distributions due to impinging-shock–expansion-corner interaction, $\bar{x}_{sh} = 1$.

rose to the inviscid level as discussed previously. However, the surface pressure distribution with the incident shock upstream of the expansion corner showed a gradual increase ahead of the inviscid pressure jump, Fig. 35. The proximity of the expansion corner prevented the pressure from reaching the downstream, inviscid shock level, with the stronger expansion suppressing the rise more effectively. In the subsequent expansion, the surface pressure reached the final inviscid value in a relatively shorter distance of $\bar{x}_D = 1$–2 compared against a pure expansion corner flow where $\bar{x}_D = 5$–6, Fig. 21. Further, the mutual shock–expansion interaction was evident in a decrease of the downstream influence with increasing shock strength p_F/p_1.

For a boundary layer with shock impingement right at the corner, the surface pressure distributions are displayed in Fig. 36. The surface pressure distributions appeared similar to those on a flat plate, see Figs. 32 and 33. The corner attenuated the pressure rise due to the impinging shock.[31] For the $\alpha = 4.25°$ and $\beta = 2°$ case where the shock was almost cancelled by the expansion ($p_F/p_1 = 0.95$) the surface pressure downstream of the corner did not decay to the inviscid level within the measurement zone, Fig. 36*b*.

When the shock impinged downstream of the corner, the surface pressure distributions showed a smaller upstream influence compared to those with shock impingement ahead and on the corner, Fig. 37. The downstream shock was strong enough to overcome the inviscid pressure drop. In addition, the downstream surface pressure showed an overshoot compared with inviscid pressure levels. This overshoot may, however, be due to errors in accurately measuring the shock generator angle.

The upstream influence scale is summarized in Fig. 38, in which the normalized upstream influence x_u/δ_o^* is plotted for the twelve test cases. The upstream influence was larger with stronger shocks as expected. When the shock impinged downstream of the corner, the upstream influence decreased, particularly for $\beta = 4°$, due to the mutual shock–expansion interaction. Further, the upstream influence for a given shock generator decreased with a stronger expansion. In other words, a stronger expansion further weakened the pressure rise associated with the incident shock. The mutual interaction between the expansion and the shock wave are discussed in more detail next through an analysis of pressure fluctuation data.

Figs. 39–44 show the rms distribution of the surface pressure fluctuations. The local rms value σ_p is normalized by the local surface pressure p_w, the upstream rms value $\sigma_{p,o}$ and the freestream dynamic pressure q_∞. The pressure fluctuation with the impinging shock upstream of the corner (Figs. 39*a* and 40*a*) showed some similiar features, e.g., the "peak" rms pressure fluctuation associated with the strong intermittent behavior of the interaction, a damping downstream of the expansion corner and a slight increase further downstream at $\bar{x} = 3.3$ and 4.2 for $\alpha = 2.5°$ and $4.25°$ respectively. This slight increase of pressure fluctuation may imply the start of a recovery to a new equilibrium turbulent state. The shock appeared to enhance the recovery and moved the recovery location closer to the corner since the expansion corner flow without shock impingement did not show any peak at all. No clear

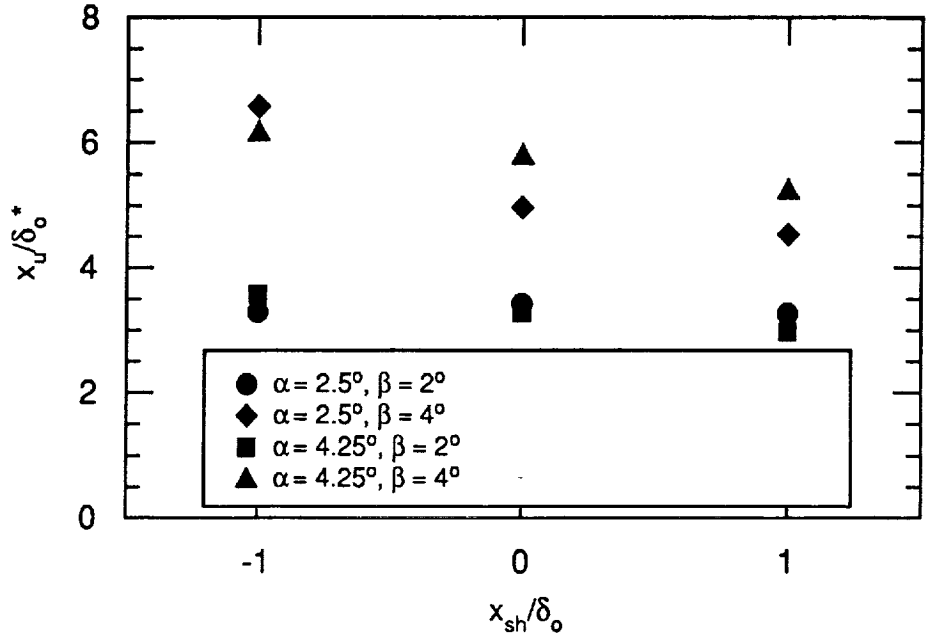

Figure 38: Upstream influence due to shock impingement near an expansion corner.

peak was discerned in the cases where the shock impinged at or downstream of the corner, Figs. 41*a* and 42*a*. This may be because the recovery was occurring further downstream. Further, the fluctuations can be compared with that of the flat plate flow with shock impingement. The appropriate comparison is with either $\sigma_p/\sigma_{p,o}$ or σ_p/q_∞. For example, σ_p/q_∞ showed a decrease downstream of the expansion corner, Fig. 40*c*. At $\bar{x} = 2.5$, σ_p/q_∞ was 0.0015 and 0.0038 for $\beta = 2°$, 4° respectively, and these were only about 50 percent of the flat plate value (Fig. 30). The attenuation induced by the favorable pressure gradient is clearly evident.

Furthermore, the characteristic shape of the rms pressure distribution was basically the same when the incident shock impinged right at the expansion corner as when the shock impinged ahead of the corner, Figs. 41*a* and 42*a*. However, the attenuation of the reflected shock by the expansion corner tended to reduce the rms peak. For $\alpha = 4.25°$ and $\beta = 2°$, $(\sigma_p/p_w)_{max}$ was about 20 percent below the peak value for the impinging shock upstream of the corner.

When the shock impinged downstream of the corner, the rms pressure distributions also showed similiar shapes as those discussed above, Figs. 43*a* and 44*a*. However, for the weakest combination, with $\alpha = 2.5°$ and $\beta = 2°$, the influence of the expansion is not completely clear. Also, Figs. 43*b* and 44*b* show that the recovery of the boundary layer was further downstream compared with those of shock impingement upstream of the corner. A reduction of interaction length was seen and this implied that the

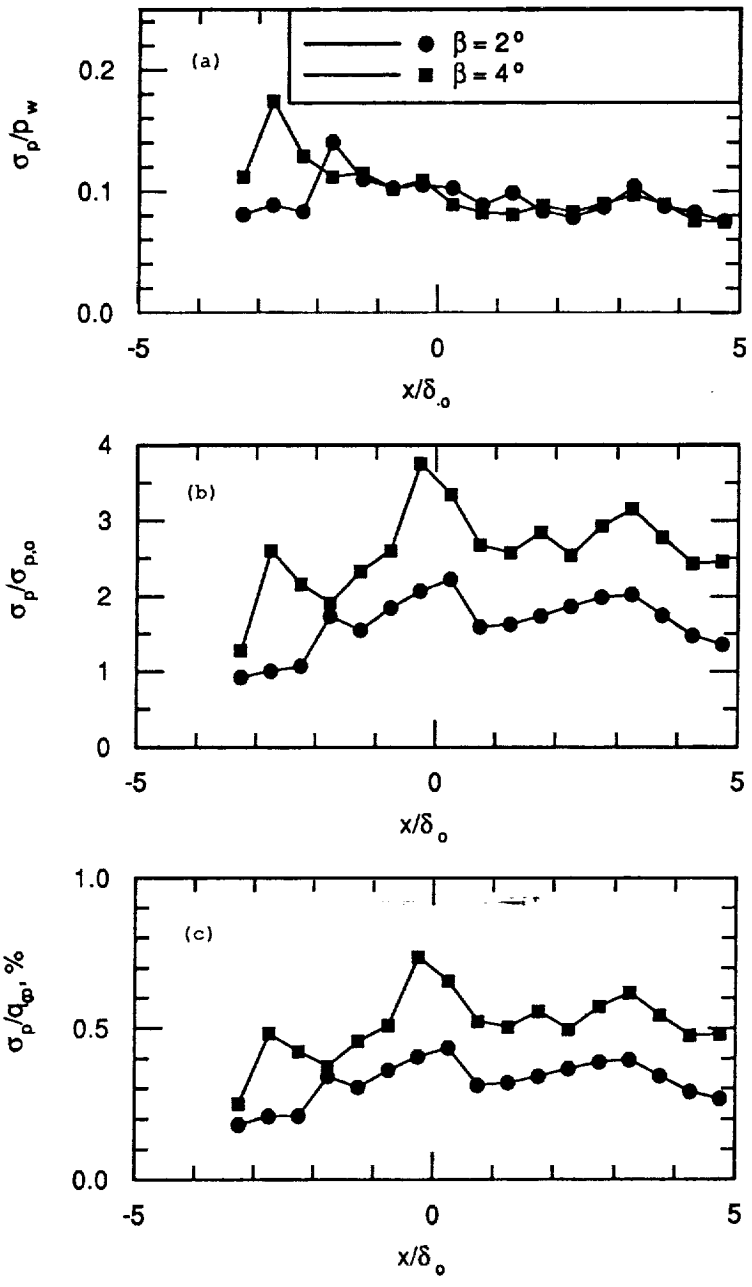

Figure 39: Pressure fluctuation distributions, $\alpha = 2.5°$, $\bar{x}_{sh} = -1$.

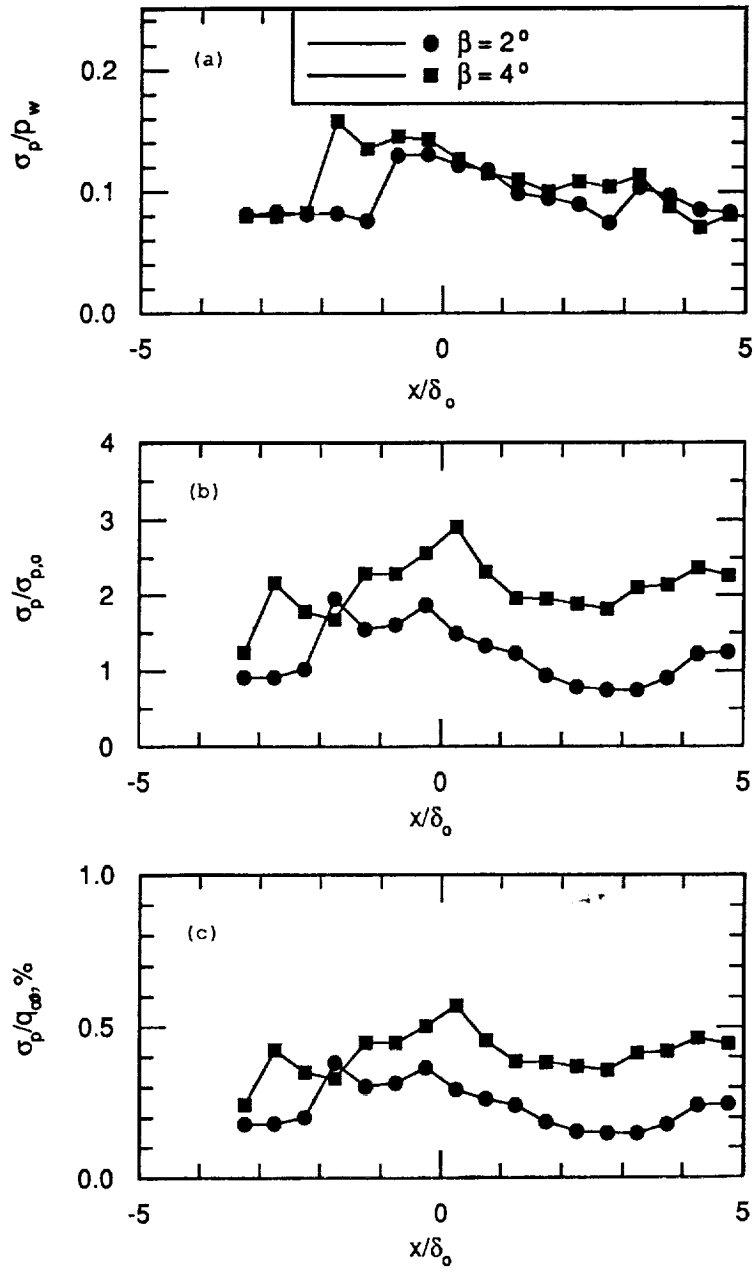

Figure 40: Pressure fluctuation distributions, $\alpha = 4.25°$, $\bar{x}_{sh} = -1$.

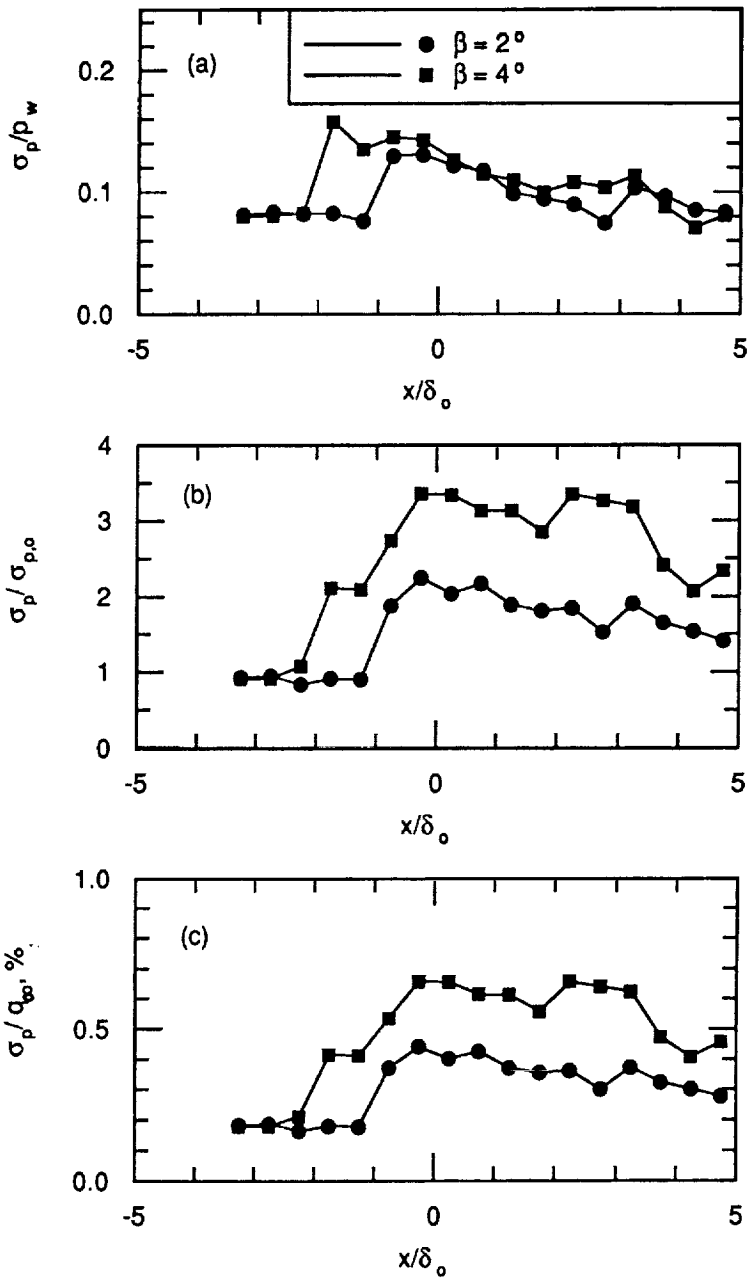

Figure 41: Pressure fluctuation distributions, $\alpha = 2.5°$, $\bar{x}_{sh} = 0$.

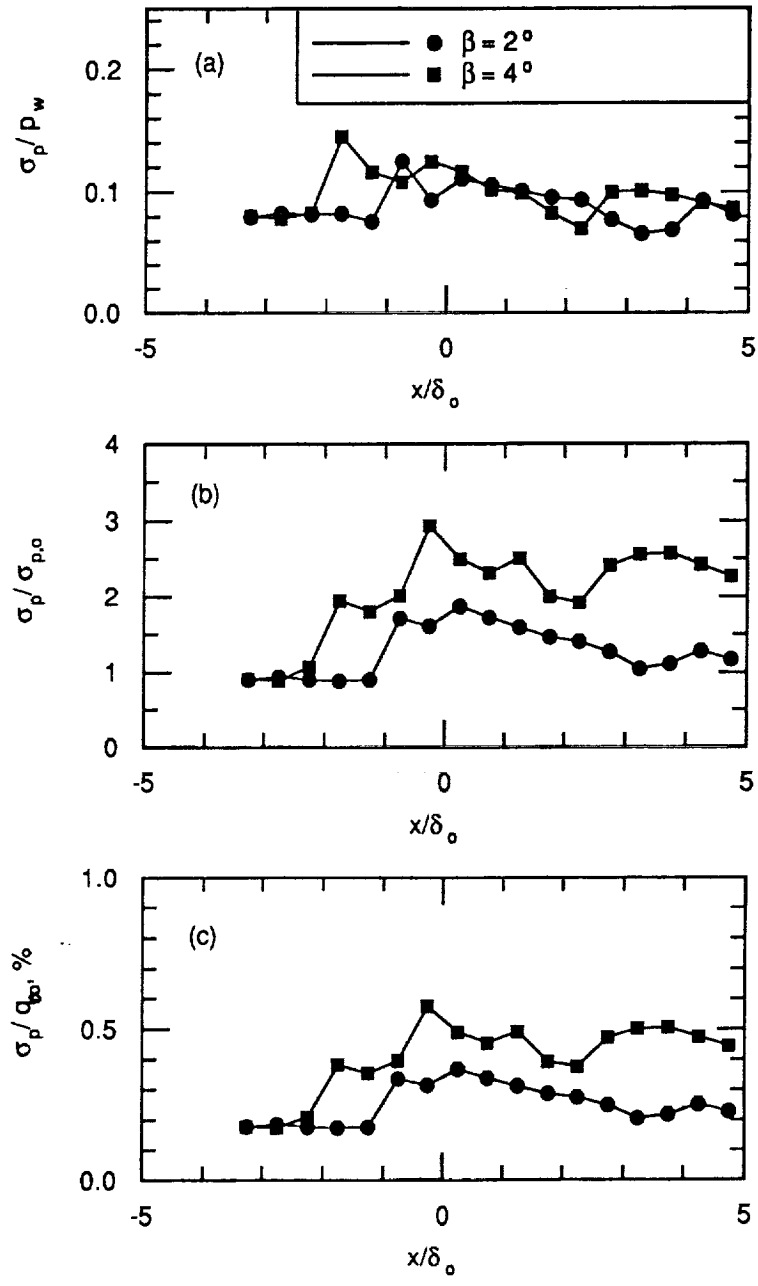

Figure 42: Pressure fluctuation distributions, $\alpha = 4.25°$, $\bar{x}_{sh} = 0$.

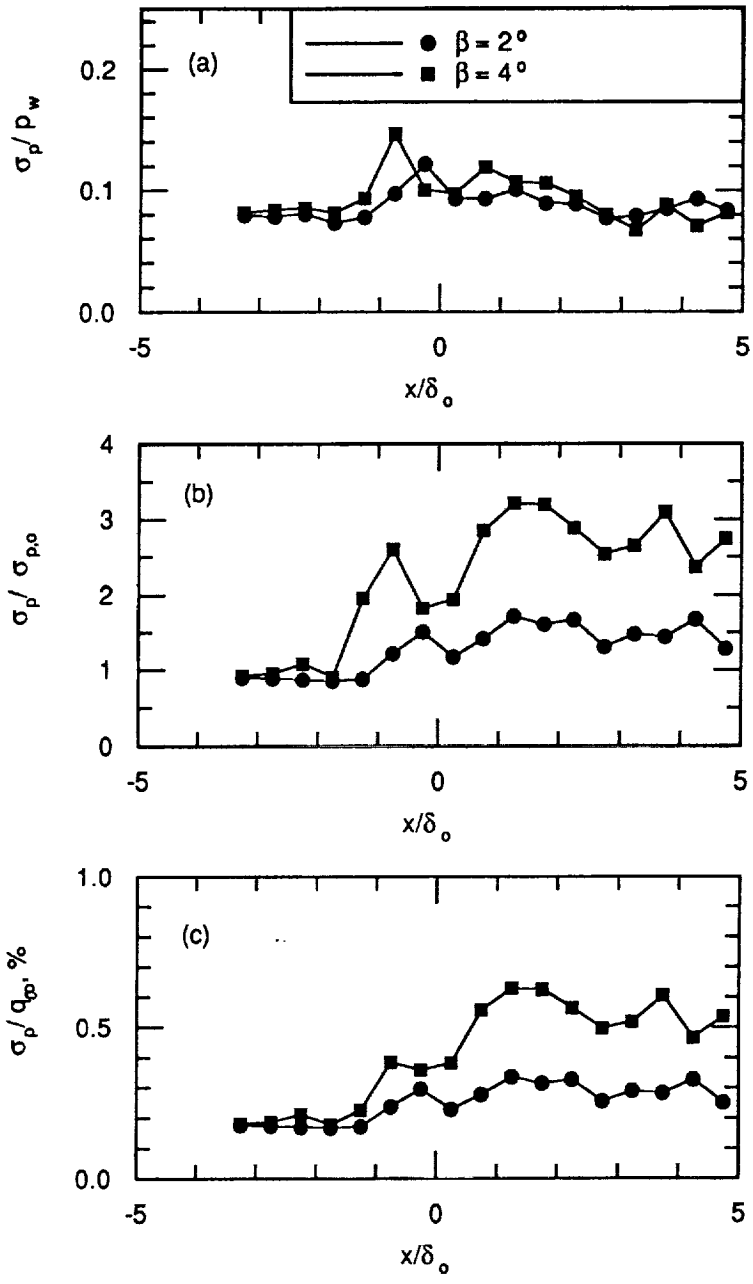

Figure 43: Pressure fluctuation distributions, $\alpha = 2.5°$, $\bar{x}_{sh} = 1$.

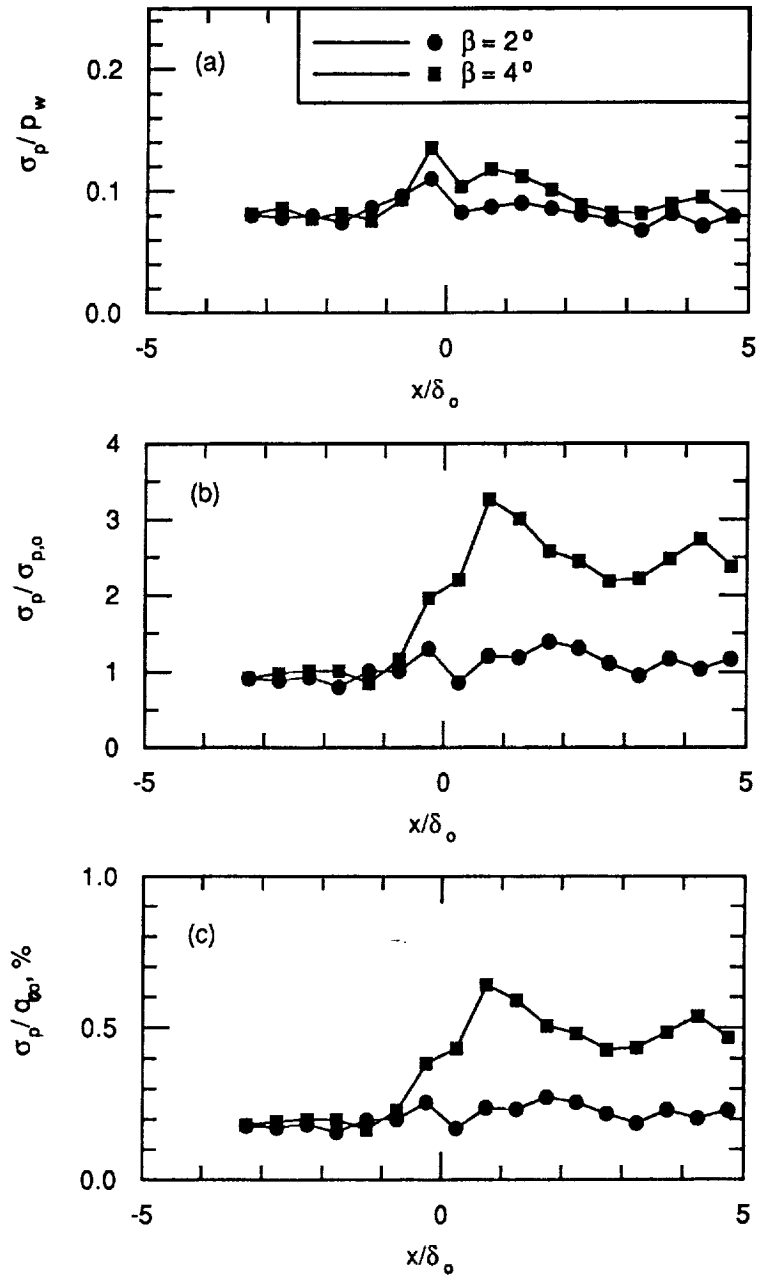

Figure 44: Pressure fluctuation distributions, $\alpha = 4.25°$, $\bar{x}_{sh} = 1$.

influence of the incident shock was weakened by the expansion fan that laid ahead. Further, it is interesting to note that Chew's study[31] indicated an independence between the expansion and incident shock flows as $\bar{x}_{sh} \approx 1.5$, in which the pressure drop due to the expansion fan is completed ahead of the impinging shock. In the present hypersonic flow, the surface pressure decreased in a more uniform fashion due to the highly-swept expansion fan and there was a larger degree of interference between the shock and the expansion.

Examples of normalized pdfs for the shock–expansion interaction are plotted in Figs. 45 and 46. The pdfs showed a highly skewed upstream signal and a bimodal distribution of pressure fluctuation further downstream which indicated the intermittent nature of the signals due to shock motion. Also, the pdfs of the $\beta = 4°$ case showed a further upstream propagation of disturbances than that of the $\beta = 2°$ case. This indicated a larger upstream influence for a stronger shock strength.

Pitot pressure profiles of shock impingement at a 2.5° expansion corner are displayed in Fig. 47. Pressure and distance are normalized by the pitot pressure $p_{pit,e}$ at the boundary layer edge and the local boundary layer thickness δ respectively. These profiles can be compared with those of a flat-plate flow with impinging shock (Fig. 34). The profiles for both expansion corners showed less distortion than those of the flat plate. The decreased distortion was due to the neutralization of the reflected shock waves by the expansion.

4 Conclusions and Recommendations for Further Study

4.1 Conclusions

4.1.1 Fin Interactions

The fin-induced, shock wave, turbulent boundary-layer interaction at Mach 8 was found to be highly swept and separated even at the lowest fin angle of $\alpha = 5°$. The large sweep implied a very rapid deflection of the surface flow. The spanwise extent of the interaction was large in comparison to the inviscid shock location. In all the cases studied, separation occurred almost immediately following interaction onset. Attachment occurred very near the base of the fin. Evidence of secondary separation was found in the interaction generated by $\alpha = 10$–$20°$ fins. The surface pressure distribution appeared flat for a large extent, almost immediately from the upstream influence to the vicinity of the inviscid shock location, where the surface pressure increased rapidly. However, the surface pressure did not reach the inviscid downstream value unlike supersonic interactions.

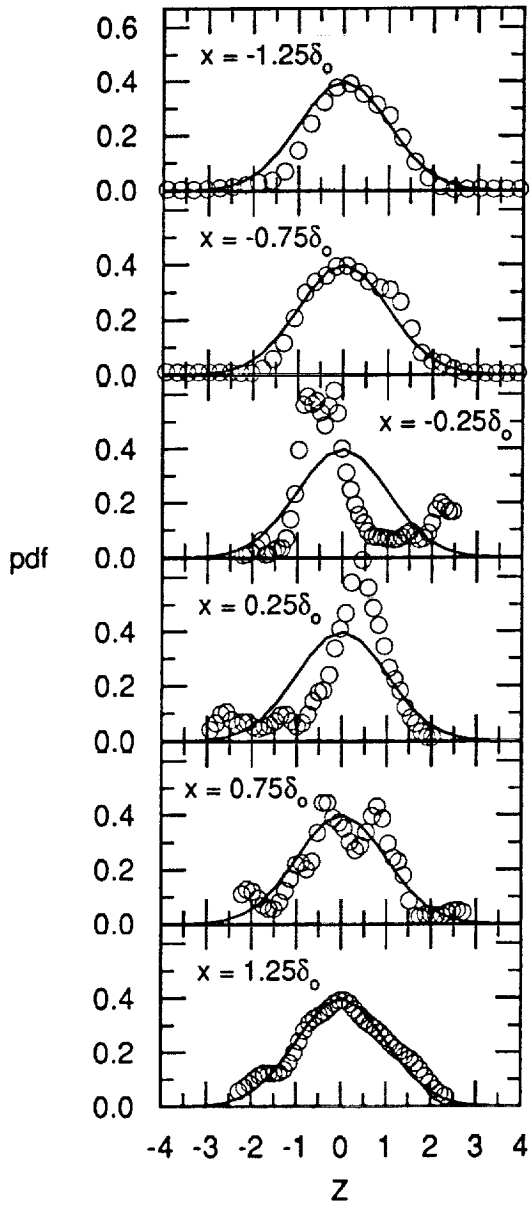

Figure 45: PDFs of shock impingement downstream of corner, $\alpha = 2.5°$, $\beta = 2°$, $\bar{x}_{sh} = 1$.

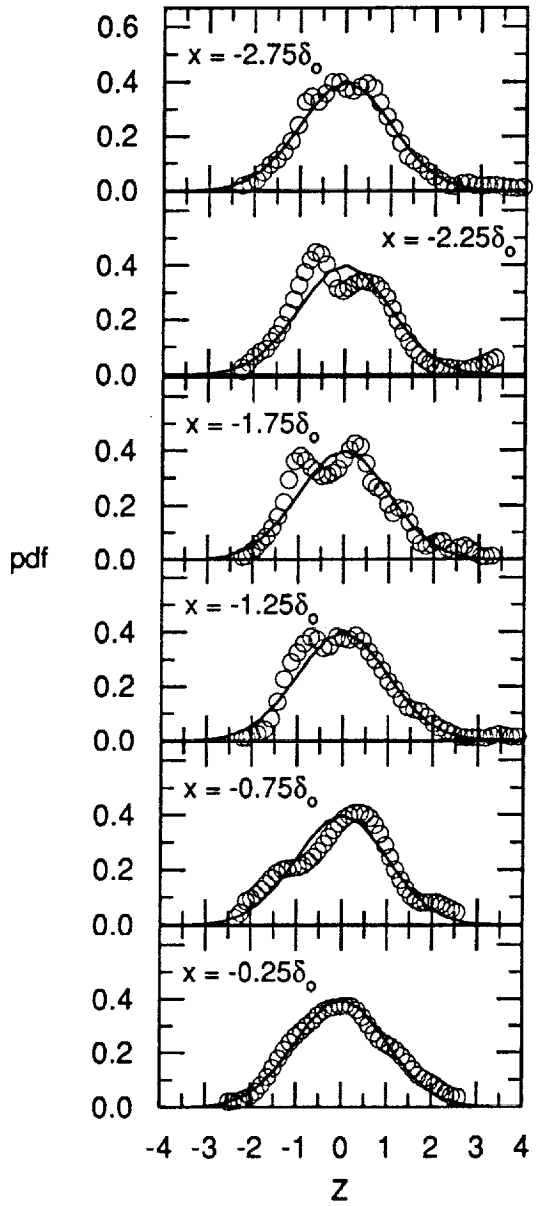

Figure 46: PDFs of shock impingement downstream of corner, $\alpha = 2.5°$, $\beta = 4°$, $\bar{x}_{sh} = 1$.

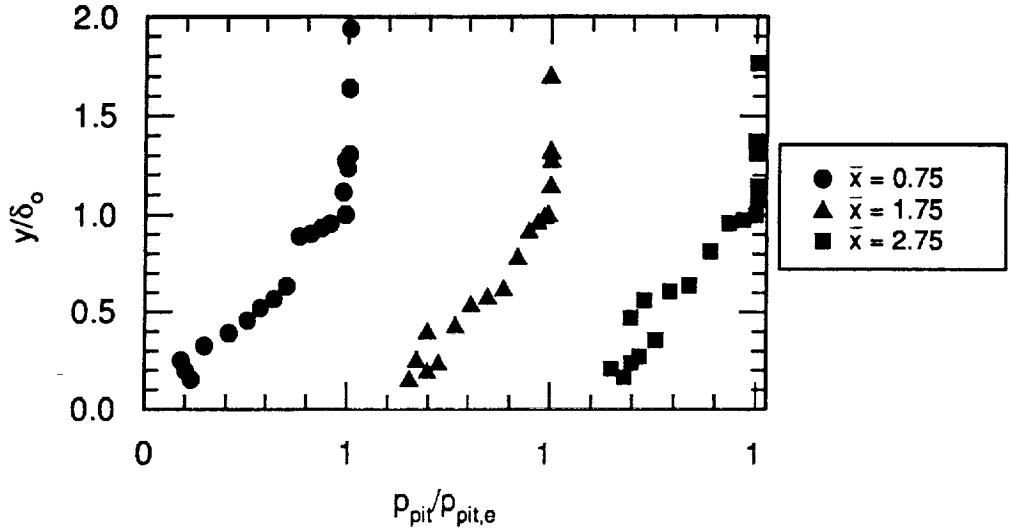

(a) $\alpha = 2.5°$, $\beta = 2°$.

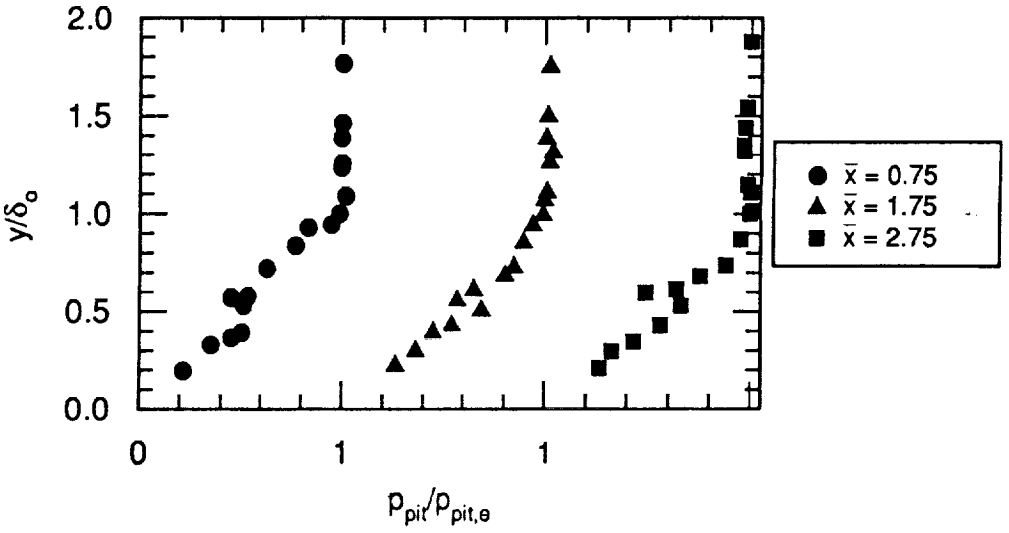

(b) $\alpha = 2.5°$, $\beta = 4°$.

Figure 47: Pitot pressure profiles of shock impingement at a 2.5° expansion corner.

4.1.2 Expansion Corner Flows

A downstream influence was identified based on mean surface pressure distributions and was found to scale with a hypersonic similarity parameter. An examination of the surface pressure fluctuations of hypersonic turbulent flow downstream of small expansion corners revealed that they were normally distributed through the expansion process but were severely attenuated. The pressure fluctuations indicated that there was no recovery to an equilibrium turbulent flow within four to six incoming boundary-layer thicknesses downstream even though the mean pressures reached downstream inviscid values within that distance. The fluctuations were convected with a velocity comparable to that on a flat plate and these fluctuations maintained their identities longer for stronger expansions. The large damping of the pressure fluctuations, even by small corner angles, may be exploited in fatigue design.

4.1.3 Shock Impingement Near Expansion Corners

The highly swept shock–expansion system examined in this study interacted closely unlike that in a supersonic flow. Depending on whether the shock impinged ahead or behind an expansion corner, the mutual interaction showed different characteristics. If the shock impinged ahead of the corner, the upstream portion of the interaction was oblivious of the presence of the corner. Therefore, structural features such as the upstream influence, measured from the inviscid shock impingement location, were identical to that arising from impingement on a flat plate. The expansion corner drastically modified the downstream flow in not only preventing further increases in pressure but also in damping out the surface pressure fluctuations. When the shock impinged behind the corner, the shock was able to overcome the expansion process in preventing the surface pressure from dropping. The downstream influence, measured from the corner, was shorter. The reduction of the downstream influence and the rms peak were also evident in the rms pressure distribution.

4.2 Recommendations for Further Study

4.2.1 Fin Interactions

The fact that the surface pressures did not reach the inviscid downstream value may be worth investigating. It would be helpful to extend the wall measurements to include measurements on the fin surface to provide more insight on the interaction structure. Off-surface data, e.g., from flow visualization, would verify the flowfield behavior inferred from the surface measurements.

4.2.2 Expansion Corner Flows

The hypersonic similarity parameter identified in this study is based on a limited number of cases while the behavior of strongly expansive flows is still unknown. In

particular, whether strong expansive flows still scale according to the hypersonic similarity parameter needs investigation. Relaminarizing flows are also not well understood, especially at high speeds. Data sensitive to the transition process, such as skin friction or heat transfer, should be useful in studying relaminarization. Further, although the flow appears inviscid in nature and therefore relatively easy to solve by a method-of-characteristics approach, it may be useful to perform a triple-deck analysis to properly characterize the physical parameters that govern expansive turbulent flows.

4.2.3 Shock Impingement Near Expansion Corners

Based on the present experiments, further work should involve stronger shocks and expansions, including cases where the shock induces boundary layer separation. However, such experiments must be carefully thought out with respect to the relative position of the shock and the corner. The reason is that the separation bubble introduces additional length scales into the interaction. The effect of the expansion on the downstream flow is perhaps of greater interest than the upstream influence since the recovery process is expected to be highly dependent on the relative strengths of the shock and expansion.

Acknowledgements

The research effort would not be possible without the funding support of NASA Langley Research Center through Grant No. NAG 1-891. The author appreciates the constant encouragement and support of the project monitor, Dr. John P. Weidner. The author also gratefully acknowledges numerous useful discussions with his colleague Dr. Donald R. Wilson and the expertise of Messrs. Jim H. Holland and Gene Sloan in fabricating the models and ensuring smooth operation of the shock tunnel. Finally the author acknowledges the assistance of the graduate and undergraduate students who participated in the research and, in particular, he acknowledges the valiant efforts of Messrs. Kung-Ming Chung and Glenn Pace.

5 References

1. Anderson, J. D., Jr., "A Survey of Modern Research in Hypersonic Aerodynamics," AIAA Paper No. 84-1578, 1984.

2. Marvin, J. G., "Modeling of Turbulent Separated Flows for Aerodynamic Applications," NASA TM 84392, 1983.

3. Settles, G. S. and Dodson, L. J., "Hypersonic Shock/Boundary-Layer Interaction Database," AIAA Paper No. 91-1763, 1991.

4. Délery, J., "Shock Wave/Turbulent Boundary Layer Interaction and Its Control," *Prog. Aerosp. Sci.*, Vol. 22, 1985, pp. 209–280.

5. Délery, J. and Marvin, J. G., "Shock-Wave Boundary Layer Interactions," AGARD-AG-280, 1986.

6. Settles, G. S. and Dolling, D. S., "Swept Shock Wave/Boundary-Layer Interactions," *AIAA Prog. Astro. Aero.*, Vol. 104, 1986, pp. 297–379.

7. Settles, G. S. and Dolling, D. S., "Swept Shock/Boundary-Layer Interactions – Tutorial and Update," AIAA Paper No. 90-0375, 1990.

8. Hayes, J. R., "Prediction Techniques for the Characteristics of Fin Generated Three Dimensional Shock Wave Boundary Layer Interactions," AFFDL-TR-77-10, 1977.

9. Scuderi, L. F., "Expressions for Predicting Three-Dimensional Shock Wave-Turbulent Boundary Layer Interaction Pressures and Heating Rates," AIAA Paper No. 78-162, 1978.

10. Lu, F. K., "Initial Operation of the UTA Shock Tunnel," AIAA Paper No. 92-0331, 1992.

11. Gough, H. and Parker, J., *A Glossary of Terms Used in Heraldry*, Gale Research Co., Detroit, Michigan, 1966.

12. Wilson, D. R., "Development of the University of Texas at Arlington Aerodynamics Research Center," AIAA Paper No. 88-2002, 1988.

13. Stuessy, W. S., Murtugudde, R. G., Lu, F. K. and Wilson, D. R., "Development of the UTA Hypersonic Shock Tunnel," AIAA Paper No. 90-0080, 1990.

14. Chung, K.-M. and Lu, F. K., "Shock-Tube Calibration of a Fast-Response Pressure Transducer," AIAA Paper No. 90-1399, 1990.

15. Gibson, B. and Dolling, D. S., "Wall Pressure Fluctuations Near Separation in a Mach 5, Sharp Fin-Induced Turbulent Interaction," AIAA Paper No. 91-0646, 1991.

16. Schewe, G., "On the Structure and Resolution of Wall-Pressure Fluctuations Associated with Turbulent Boundary-Layer Flows," *J. of Fluid Mech.*, Vol. 134, 1983, pp. 311–328.

17. Dolling, D. S. and Dussauge, J. P., "Fluctuating Wall-Pressure Measurements," *A Survey of Measurements and Measuring Techniques in Rapidly Distorted Compressible Turbulent Boundary Layers*, edited by H. H. Fernholz et al., AGARD-AG-315, 1988, Chapter 8.

18. Edney, B. E., "Temperature Measurements in a Hypersonic Gun Tunnel Using Heat-Transfer Methods," *J. Fluid Mech.*, Vol. 27, 1967, pp. 503–512.

19. Kipke, K. and Hummel, D., "Untersuchungen an längsangeströmten Eckenkonfigurationen im Hyperschallbereich. Teil I: Ecken zwischen ungepfeilten Keilen," *Z. Flugwiss*, Vol. 23, 1975, pp. 417–429.

20. Tang, G.-M. and Yu, H.-R., "Experimental Investigation of the Shock Wave and Turbulent Boundary Layer Interaction Induced by a Cylindrical Protuberance," *Current Topics in Shock Waves: 17th Int. Symp. Shock Waves and Shock Tubes*, ed. by Y. W. Kim, AIP Conf. Proc. 208, 1990, pp. 264–269.

21. Arrington, J. P., Joiner, R. C., Jr. and Henderson, A., Jr., "Longitudinal Characteristics of Several Configurations at Hypersonic Mach Numbers in Conical and Contoured Nozzles," NASA TN D-2489, 1964.

22. Elfstrom, G. M., "Turbulent Hypersonic Flow at a Wedge-Compression Corner," *J. Fluid Mech.*, Vol. 53, 1972, pp. 113–127.

23. Chung, K.-M. and Lu, F. K., "An Experimental Study of a Cold-Wall Hypersonic Boundary Layer," AIAA Paper No. 92-0312, 1992.

24. Settles, G. S. and Lu, F. K., "Conical Similarity of Shock/Boundary-Layer Interactions Generated by Swept and Unswept Fins," *AIAA J.*, Vol. 23, No. 7, 1985, pp. 1021–1027.

25. Inger, G. R., "Spanwise Propagation of Upstream Influence in Conical Swept Shock Boundary-Layer Interactions," *AIAA J.*, Vol. 25, No. 2, 1987, pp. 287–293.

26. Knight, D. D. and Badekas, D., "On the Quasi-Conical Flowfield Structure of the Swept Shock Wave-Turbulent Boundary Layer Interaction," AIAA Paper No. 91-1759, 1991.

27. Anderson, J. D., Jr., *Hypersonic and High Temperature Gas Dynamics*, McGraw-Hill, New York, 1989.

28. Stollery, J. L. and Bates, L., "Turbulent Hypersonic Viscous Interaction," *J. Fluid Mech.*, Vol. 63, 1974, pp. 145–156.

29. Van Dyke, M. D., "The Combined Supersonic-Hypersonic Similarity Rule," *J. Aero. Sci.*, Vol. 18, 1951, pp. 499–500.

30. Bloy, A.W., "The Expansion of a Hypersonic Turbulent Boundary Layer at a Sharp Corner," *J. Fluid Mech.*, Vol. 67, 1975, pp. 647–655.

31. Chew, Y.T., "Shockwave and Boundary Layer Interaction in the Presence of an Expansion Corner," *Aeron. Quart.*, Vol. XXX, 1979, pp. 506–527.

32. Goldfeld, M.A., "On the Reverse Transition of Compressible Turbulent Boundary Layer in a Transverse Flow Around a Convex Corner Configuration," *Proc. of the IUTAM Symp. on Laminar-Turbulent Transition, July 9–13, 1984*, ed. by V. V. Kozlov, Springer-Verlag, Berlin, 1985, pp. 515–520.

33. Dussauge, J.P. and Gaviglio, J., "The Rapid Expansion of a Supersonic Turbulent Flow: Role of Bulk Dilatation," *J. Fluid Mech.*, Vol. 174, 1987, pp. 81–112.

34. Minucci, M. A. S. and Nagamatsu, H. T., "An Investigation of Hypersonic Shock Tunnel Testing at an Equilibrium Interface Condition of 4100 K: Theory and Experiment," AIAA Paper No. 91-1707, 1991.

35. Wittliff, C. E., "A Survey of Existing Hypersonic Ground Test Facilities – North America," *Aerodynamics of Hypersonic Lifting Vehicles*, Paper 1, AGARD CP-428, 1987.

36. Wendt, J. F., "European Hypersonic Wind Tunnels," *Aerodynamics of Hypersonic Lifting Vehicles*, Paper 2, AGARD CP-428, 1987.

37. Daum, F. L. and Gyarmathy, G., "Condensation of Air and Nitrogen in Hypersonic Wind Tunnels," *AIAA J.*, Vol. 6, No. 3, 1968, pp. 458–465.

38. Morrisette, E. L., Stone, D. R. and Cary, A. M., "Downstream Effects of Boundary Layer Trips in Hypersonic Flows," NASA SP 216, 1968.

39. Hopkins, E. J., Jillie, D. W. and Sorensen, V. L., "Charts for Estimating Boundary-Layer Transition on Flat Plates," NASA TN D-5846, 1970.

40. Fernholz, H. H. and Finley, P. J., "A Critical Commentary on Mean Flow Data for Two-Dimensional Compressible Turbulent Boundary Layers," AGARD-AG-253, 1980.

41. Davies, W. R. and Bernstein, L., "Heat Transfer and Transition to Turbulence in the Shock-Induced Boundary Layer on a Semi-Infinite Flat Plate," *J. Fluid Mech.*, Vol. 36, 1969, pp. 87–112.

42. Korkegi, R. H., "A Simple Correlation for Incipient Turbulent Boundary-Layer Separation Due to a Skewed Shock Wave," *AIAA J.*, Vol. 11, No. 11, 1973, pp. 1578–1579.

43. Kussoy, M. I., Kim, K.-S. and Horstman, K. C., "An Experimental Study of a Three-Dimensional Shock Wave/Turbulent Boundary-Layer Interaction at a Hypersonic Mach Number," AIAA Paper No. 91-1761, 1991.

44. Bloy, A. W. and Georgeff, M. P., "The Hypersonic Laminar Boundary Layer Near Sharp Compression and Expansion Corners," *J. Fluid Mech.*, Vol. 63, 1974, pp. 431–447.

45. Rizzetta, D.P., Burgraff, O.R. and Jenson, R., "Triple-Deck Solutions for Viscous Supersonic and Hypersonic Flow Past Corners," *J. Fluid Mech.*, Vol. 89, 1978, pp. 535–552.

46. Narasimha, R. and Viswanath, P.R., "Reverse Transition at an Expansion Corner in Supersonic Flow," *AIAA J.*, Vol. 13, No. 5, 1975, pp. 693–695.

47. Smith, D. R. and Smits, A. J., "The Rapid Expansion of a Turbulent Boundary Layer in a Supersonic Flow," *Theor. and Comput. Fluid Dyn.*, Vol. 2, 1990, pp. 319–328.

48. Bendat, J. S. and Piersol, A. G., *Random Data*, 2nd ed., Wiley, New York, 1986.

49. Laganelli, A. L., Martellucci, A. and Shaw, L. L., "Wall Pressure Fluctuations in Attached Boundary-Layer Flow," *AIAA Journal*, Vol. 21, No. 4, 1983, pp. 495–502.

50. Narasimha, R. and Sreenivasan K. R., "Relaminarization of Fluid Flows," *Advances in Applied Mechanics*, Vol. 19, 1979, pp. 221–309.

51. Raman, K. R., "Surface Pressure Fluctuations in Hypersonic Turbulent Boundary Layers," NASA CR-2386, 1974.

52. Reda, D. C. and Murphy, J. D., "Shock Wave/Turbulent Boundary-Layer Interactions in Rectangular Channels," *AIAA J.*, Vol. 11, No. 2, 1973, pp. 139–140.

53. Settles, G. S., Perkins, J. J. and Bogdonoff, S. M., "Upstream Influence Scaling of 2-D and 3-D Shock/Turbulent Boundary-Layer Interactions at Compression Corners," AIAA Paper No. 81-0334, 1981.

54. Dolling, D. S. and Or, C. T., "Unsteadiness of the Shock Wave Structure in Attached and Separated Compression Ramp Flows," *Exp. Fluids*, Vol. 3, 1985, pp. 24–32.

55. Gramann, R. A. and Dolling, D. S., "Dynamics of Separation and Reattachment in a Mach 5 Unswept Compression Ramp Flow," AIAA Paper No. 90-0380, 1990.

56. Muck, K.-C., Andreopoulos, J. and Dussauge, J., "Unsteady Nature of Shock-Wave/Turbulent Boundary-Layer Interactions," *AIAA J.*, Vol. 26, No. 2, 1988, pp. 179–187.

57. Tran, T. T., "An Experimental Investigation of Unsteadiness in Swept Shock Wave/Turbulent Boundary Layer Interaction," Ph.D. Dissertation, Princeton Univ., 1987.

58. Green, J. E., "Reflection of an Oblique Shock Wave by a Turbulent Boundary Layer," *J. Fluid Mech.*, Vol. 40, 1970, pp. 81–95.

59. Xerikos, J., Rose, W. C., Rawlinson, E. G. and Harris, T. B., "Measurement of Mean and Fluctuating Flow Properties in Hypersonic Shear Layer," AIAA Paper No. 90-1409, 1990.

A Nomenclature

$\bar{D}_c$ = normalized convection distance, $\tau\, U_c/\delta_o$

f = frequency

K = $M_\infty \alpha$, hypersonic similarity parameter

M = Mach number

M_n = $M_\infty \sin\beta_o$, Mach number normal to inviscid shock trace

p = pressure

q = dynamic pressure

$R_{pp}(\xi,\, \tau)$ = normalized wall pressure space-time correlation between transducers 1 and 2, $[\frac{1}{N}\sum_{n=1}^{N} p_1'(t_n)\, p_2'(t_n+\tau)]/[\sigma_{p_1}\, \sigma_{p_2}]$

Re = unit Reynolds number

s = distance measured from the fin apex

T = temperature

U = velocity

U_τ = friction velocity, $\sqrt{\tau_w/\rho_w}$

x = coordinate along the surface of the corner

$\bar{x}$ = x/δ_o

α = fin, shock generator or expansion corner angle

β = angle measured from incoming freestream direction centered at the virtual origin; also, external shock generator angle

γ = specific heat ratio

δ = boundary layer thickness

θ = momentum thickness

ν = kinematic viscosity

ξ = pressure ratio across a shock wave; also, transducer spacing

σ = surface flow deflection angle from the incoming stream

σ_p = standard deviation of surface pressure fluctuations, $[\sum_{n=1}^{N}(p(t_n) - < p >)^2/N]^{1/2}$

τ = wall shear stress or time delay in auto- and cross-correlations

Subscripts

c = convective

D = downstream influence

F = downstream of inviscid shock in two-dimensional, shock boundary-layer interactions

o = stagnation condition, inviscid shock trace on test surface or undisturbed conditions at the corner location

w = wall

1, 2 = upstream and downstream conditions of Prandtl-Meyer expansion or of inviscid shock

∞ = incoming freestream or incoming static value

Superscripts

$\bar{(\,)}$ = normalized by undisturbed boundary layer thickness at the corner
$(\,)'$ = fluctuating component of surface pressure